Applied Energy 325 (2022) 119653

Contents lists available at ScienceDirect

Applied Energy

journal homepage: www.elsevier.com/locate/apenergy

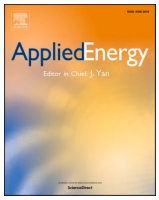

Development and performance comparison of a modified glazed CPC hybrid solar collector coupled with a bifacial PVT receiver

Diogo Cabral

Department of Building Engineering, Energy Systems and Sustainability Science, University of Gävle, Kungsbäcksvägen 47, 801 76 Gävle, Sweden

HIGHLIGHTS

- An optical efficiency of 62% has been achieved for two reflector geometry versions.
- Experimental and theoretical η_0 reached a deviation of <1% at normal incidence.
- U-values of around 5 W/m^2.K have been achieved due to a lower concentration factor.
- The CPVT collector reached an increase in electrical efficiency of +16.5%.
- At high temperatures, CPVTs have lower annual energy yields than PV + ST systems.

ARTICLE INFO

Keywords:
Glazed CPC-PVT hybrid solar collector
Collector testing
Bifacial PVT receiver
Incidence Angle Modifier

ABSTRACT

Innovative concentrating PVT solar collector concepts based on a CPC geometry concept were developed to outperform the asymmetric Solarus CPVT collector and therefore decrease the energy/performance gap between CPVT and PV/ST solar collectors.

The updated reflector geometry proved to be the most suitable reflector geometry for CPVTs, where the electrical peak efficiency per gross area reached 10.6%, which is +16.5%$_{rel}$ higher than the electrical peak efficiency of the Solarus CPVT. Optical efficiencies of $\eta_0 = 62.3\%$ and $\eta_0 = 61.8\%$ for CPC 1 and CPC 2 have been achieved, respectively.

A PV module (0.5 m^2) combined with an ST solar collector (0.5 m^2) system to be able to deliver the same overall energy yield as the newly developed CPVT collector (1 m^2) requires on average +0.02 m^2 (at 45 °C), −0.06 m^2 (at 55 °C) and −0.15 m^2 (at 65 °C) of installed area, for a wide range of latitudes.

A CPC-PVT system to increase its competitiveness requires a material cost reduction and at the same time an increased overall efficiency. Nevertheless, the energy/performance gap between a system composed of PV + ST technologies and a CPC-PVT decreased significantly.

1. Introduction

1.1. Photovoltaic-thermal solar collectors' literature review

Solar energy systems are progressively increasing their installed capacity due to subsidies and also due to solar system efficiency growth. Higher efficiencies and economic competitiveness increase annually, which leads to more investment and a sustainable energy mix.

Solar radiation can be harvested through a photovoltaic (PV) system for electricity generation, which have electrical efficiencies closer to the Shockley-Quiesser efficiency limit [1], and a solar thermal (ST) system for heat generation. The PV cell efficiency has grown exponentially in the past decades, and currently, the record lab measurement is around 27% for mono-crystalline and 22% for multi-crystalline silicon wafer-based technology [2]. Additionally, the highest lab efficiency for thin-film technologies, namely CIGS and CdTe, is 23% and 21%, respectively. The record lab cell efficiency for Perovskite is set at 22% [3]. Over the last decades, several new technologies emerged, that couples ST absorbers with PV cells (presented in [4–11], allowing the photovoltaic-thermal (PVT) solar collectors to reach higher combined electrical and thermal (per unit area) efficiencies. The thermal coupling of PV cells with ST absorbers aids the thermal energy harvesting through a heat transfer cooling (HTF) fluid that cools down the PV cells below the operating temperature of standard PV modules, which increases the electrical performance [12], as well as decreasing the required

E-mail address: diogo.cabral@hig.se.

https://doi.org/10.1016/j.apenergy.2022.119653
Received 22 February 2022; Received in revised form 25 June 2022; Accepted 7 July 2022
Available online 18 August 2022

Nomenclature

Symbol

A	Absortance
θ_c	Acceptance half-angle [°]
T_a	Ambient temperature [°C]
θ	Incidence angle [°]
$A_{aperture}$	Aperture area [m^2]
G_{beam}	Beam irradiance [W/m^2]
C_{bottom}	Bottom concentration factor [–]
A_{cell}	Cell area [m^2]
A_c	Collector area [m^2]
η	Collector efficiency [%]
T_{in}	Collector inlet temperature [°C]
h	Collector height [mm]
T_m	Collector mean temperature [°C]
T_{out}	Collector outlet temperature [°C]
P	Collector output power [W/m^2]
C_i	Concentration factor [–]
$G_{diffuse}$	Diffuse irradiance [W/m^2]
d	Discount rate [–]
$\eta_{el\_col.}$	Electrical collector efficiency [%]
$\eta_{elect\_diff.}$	Electrical efficiency for diffuse radiation [%]
$\eta_{elect.}$	Electrical peak efficiency [%]
$\eta_{elect.\_beam}$	Electrical peak efficiency for beam radiation [%]
$\eta_{elect.\_STC}$	Electrical peak efficiency for standard testing conditions [%]
P_{el}	Electrical power output [W/m^2]
c_1	First-order heat loss coefficient at (t_m - t_a) = 0 [W/m^2.K]
f	Focus length [mm]
G_{global}	Global solar radiation [W/m^2]
A_{gross}	Gross area [m^2]
U_1	Heat loss coefficient [W/m^2.K]
Q	Instantaneous collector output power [W]
d	Market discount rate [%]
$\dot{m}$	Mass flow rate [$kg/s.m^2$]
$\rho.V$	Mass of substance [g/cm^3]
P_{mpp}	Maximum output power [W]
$\theta_{,NS}$	North-south projection angle [°]
V_{oc}	Open-circuit voltage [V]
η_{opt}	Optical efficiency from I_{sc} measurements [%]
η_{PVT}	Overall PVT efficiency [%]
η_0	Peak collector efficiency at ΔT = 0 K [–]
ΔP	Pressure interval [Bar]
$A_{reflector}$	Reflector area [m^2]
a'	Receiver size [mm]
I_{sc}	Short circuit current [A]
$I_{sc,\ measured}$	Short circuit current (measured) [A]
$I_{sc,\ standard\ module}$	Short circuit current (standard module) [A]
ρ	Solar reflectance [–]
τ	Solar transmittance [–]
T_{Ref_STC}	Standard testing conditions reference temperature [°C]
c_p	Specific heat [J/K]
Q_{el}	Specific electrical power output [W/m^2]
Q_{th}	Specific thermal power output [W/m^2]
G_{STC}	Standard testing condition irradiance [W/m^2]
c_2	Temperature dependence of heat loss coefficient [$W/m^2.K^2$]
ΔT	Temperature interval [°C]
$\eta_{opt,theo.}$	Theoretical optical efficiency [%]
$\eta_{th\_diff.}$	Thermal efficiency for diffuse radiation [%]
V	Volume [L]
n	Years

Subscripts

BIPV	Building Integrated PV
CPVT	Concentrating Photovoltaic-Thermal
CPC	Compound Parabolic Collector
FIPV	Façade Integrated PV
HTF	Heat Transfer cooling Fluid
IAM	Incidence Angle Modifier
$IAM_{Long.}$	Longitudinal Incidence Angle Modifier
$IAM_{Transv.}$	Transversal Incidence Angle Modifier
IEA	International Energy Agency
LCPVT	Low Concentrating Photovoltaic-Thermal
PC	PowerCollector
PV	Photovoltaic
PVT	Photovoltaic-Thermal
SHC	Solar Heating and Cooling
SS	Steady-state method
ST	Solar thermal

installation area.

Werner and Spörk-Dür (2020) presented the global PVT solar collector market development and respective trends for 2019, in which the total area installed was set at around 1.2×10^6 m^2 (e.g. 675×10^3 m^2 in Europe, 281×10^3 m^2 in Asia, 134×10^3 m^2 in China and 70×10^3 m^2 for the rest of the world). Unglazed water collectors are the most disseminated PVT technology with the largest market share of 55%, followed by air collectors (43%) and covered water collectors (2%). Furthermore, 86% of the PVT installations were dedicated to solar air (pre)heating of buildings, followed by 7% for Domestic Hot Water (DHW) for single-family households and the remaining 7% for DHW and space heating (i.e. multifamily houses, hotels, hospitals, swimming pools, and district heating). Currently, France has around 42% of the total installed capacity of PVT systems, whereas South Korea has around 24%, China 11% and Germany with approximately 10%. Moreover, an annual global growth of around +9% on average has been registered in the year 2018 and 2019, which was driven by a growth rate of +14% registered in Europe with an increased installed capacity of around 13 MW_{peak}. Corresponding to a total of 0.935 GW_{peak}, which can be divided into 712 MW_{th} and 235 MW_{el}. A market data based on 36 PVT manufacturers presented a constant growth of around 9% on average in the last two years.

The cumulated ST capacity in operation in 2020 was 501 GW_{th}, which results in a market decrease of 4% when compared to the previous year of 2019. ST installed capacity trailed behind wind power installed capacity of 743 GW_{el} and photovoltaics 708 GW_{el} (i.e. PV market increment of 18%), corresponding to +125 GW_{el} of installed capacity [13].

Furthermore, the increasing interest in Building Integrated PV (BIPV) and Façade Integrated PV (FIPV), and the developments in the heat pump technology generates several alternatives for PVT applications. Therefore, in 2018, under the management of the International Energy Agency (IEA) Solar Heating and Cooling (SHC) programme, a task force composed of several experts in PV, ST and PVT technology has been initiated under the IEA-SHC Task 60: 'Application of PVT collectors. The IEA-SHC task 60 focuses on the improvement of performance characterization and modelling of PVT collectors and systems [14]. Typically, the PVT thermal performance characterization is tested according to the international standard for ST collectors ISO 9806:2017 [15] and the electrical performance according to IEC standards [16]. Moreover, the PVT solar collectors can apply for the Solar Keymark certification with specific guidelines, where the thermal performance is

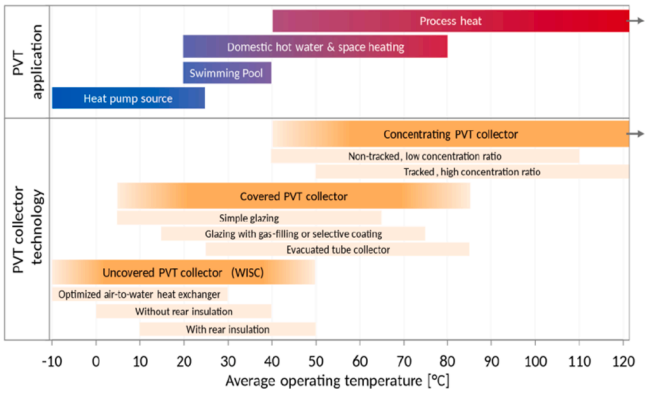

Fig. 1. Map of PVT technologies and applications per operating temperature [17].

performed with synchronous thermal and electrical generation under maximum power point conditions, as the heat and electricity influence each other. Therefore, Lämmle et al. [17] presented and allocated (in a schematic view as the one presented in Fig. 1) each PVT collector technology according to their specific operating temperature ranges, system layout, design (glazed, unglazed, and concentrating), and their heat transfer medium (air and water, for commercial systems).

The operating temperature of a specific system depends on the requirements of the heat supply system for DHW and space heating. Moreover, depending on the type of HTF, PVT technologies can be segmented into several categories [18], such as PVT air collector (e.g. space heating systems and agricultural processes) and PVT liquid collector (e.g. domestic and industrial space heating and cooling systems, water heating and desalination systems, and food processing systems).

Additionally, the generality of the PVT water collectors and ST collectors can be divided into their range of applications such as [17]:

- Low-temperature applications (~27–35 °C) including swimming pool heating or spas, while operating temperatures up to 50 °C are required for space heating;
- Medium-temperature applications for temperatures up to 80 °C (e.g. glazed or evacuated tube collectors);
- High-temperature applications for temperatures >80 °C (e.g. high-efficiency flat-plate or concentrator collectors).

1.2. PVT and CPVT solar collectors: advantages and disadvantages

Due to the newest commercial interest in PVT solar collectors, it is essential to compare the properties of PVT with standard ST and PV solar collectors. The main benefits of PVT collectors, when compared to PV and ST, are (1) the possibility of increasing cell efficiency by reducing the cell operating temperature [19], when heat is extracted at low temperatures. Therefore, it is fundamental that the panel design is able to transfer the heat from the cells to the HTF efficiently as well as homogeneously; (2) the production of one unit of PVT uses fewer raw materials than an equivalent area of ST and PV panels, which is expected to enable a lower production cost in €/kWh of annually produced heat power; (3) reduction of the installation area, which enables the deployment of more installed capacity per roof area.

On the other hand, the main disadvantages of PVT technologies are the higher complexity in both production and installation, and the reduced market share since it requires customers that simultaneously need both heat and electricity [20].

A PVT solar collector has higher heat losses than a high-efficiency ST collector, since the module surface has a high thermal emittance. Moreover, the thermal peak efficiencies for a PVT solar collector range from 48% for an unglazed PVT up to 53% for concentrating PVT, which are fairly below the 80% for standard flat plate ST collectors [21]. This phenomenon is due to the simultaneous electrical (i.e., the fraction of incident solar radiation is directly converted into electricity) and thermal generation. The lower absorptance and higher emittance of the receivers (i.e., higher optical (e.g. reflection, transmittance) and geometrical losses), in most cases, a higher thermal resistance between the PV cells and the HTF also contributes to enhance this phenomenon. On the other hand, both unglazed and glazed PVTs can compete with thin-film PV modules, but not with the high-efficiency mono-Si modules that reach electrical efficiencies of around 22%. Moreover, the LCPVT (from Solarus) can reach electrical efficiencies as high as 9.7%, which is half of a standard PV module.

Higher electrical efficiencies lead to lower thermal efficiencies, therefore a PVT collectors can either be optimized for high electrical or thermal performance.

Moreover, some PVT manufacturers combine the concept of concentration to reduce the amount of PV cell and thermal absorber material. Concentration leads to extra reflection losses from the reflector and a worse Incident Angle Modifier (IAM) profile. Additionally, it reduces the heat losses by means of less absorber area [22,23] and the number of expensive components (PV solar cells, receiver with selective surface). This way, concentration allows higher thermal efficiency at high temperatures to be achieved, although it will reduce the efficiency of the solar cells [24]. In the end, it is a trade between the positive effect of lowering the collector cost and the negative effect of lowering output per square meter of aperture area [25].

Some of the disadvantages of concentration are the bulkier appearance, higher stagnation temperatures which leads to more expensive components, and lower power density. Factors such as simplicity or aesthetics are important for solar customers; however, the most important parameter is the cost per kWh of heat and electricity produced (Gomes et al., 2014). The water temperatures obtained in hybrid PVT systems are often moderate to keep the PV cell at low temperatures due to the voltage drop with an increased temperature. If the hybrid system is to be operated at low temperatures for maximizing the electricity production, the warm water produced can be useful for floor heating and pre-heating tap water. The optical efficiency is a key to the electrical and thermal performance of a CPVT hybrid system and consequently its importance has been assessed.

1.3. Concentrating photovoltaic-thermal solar collectors

Solar collectors can be coupled with reflectors to collect irradiation from a large reflective area. The collected irradiation is focused onto an absorber which generates thermal energy at higher temperatures. It leads to higher stagnation temperatures and worse IAM profiles, as it increases optical and geometrical losses, as well as the shading effect created by the edges of the solar collector box.

Stationary low concentration factor solar collectors were not developed to reach temperatures above 120 °C [17], as it exempts the need for tracking systems due to its relatively high acceptance angles [26]. Several studies focusing on parabolic or compound parabolic troughs have been presented, yielding high thermal and electrical efficiencies as shown in Bellos and Tzivanidis [27], Valizadeh et al. [28] and Adam et al. [29].

Parabolic and Compound Parabolic Collectors (CPC) solar collectors are currently the most employed, mature and commercially proven concentrating technologies [30]. On the other hand, reflection and mismatching losses, as well as lateral shading on the edge cells, due to the collector box frame arises, which reduces the electrical performance. Lateral shading on the edge PV cells string has been reported by Bunthof et al. [31], as the main cause for decreasing the energy yield of PV arrays. In reality, stationary concentrating technologies do not provide a uniform flux distribution, which leads to uneven illumination on the PV solar cell, thus creating higher electrical resistance losses as well as material stress. Moreover, real-life surfaces have optical errors in the reflection (i.e. non-uniformities in the slope of the reflector, or

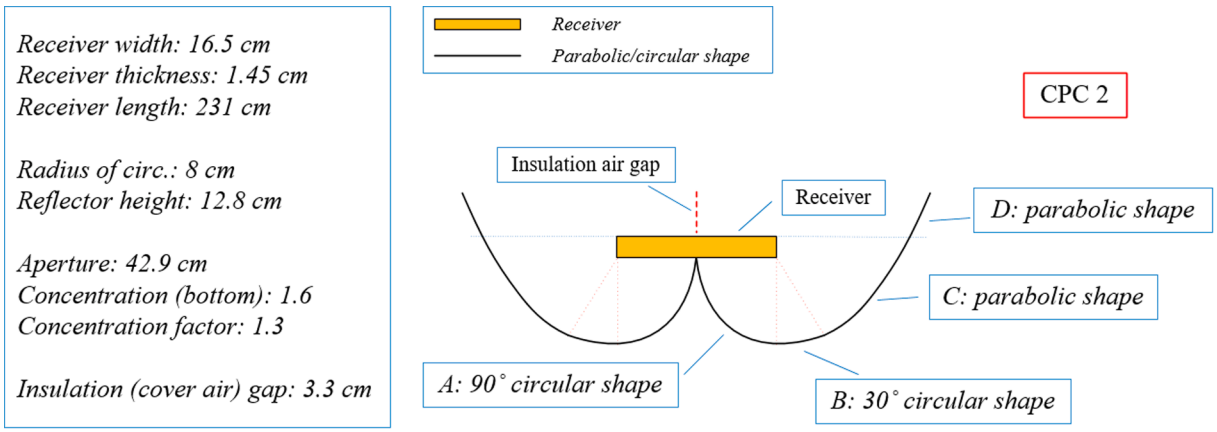

Fig. 2. CPC 2 geometry cross-section view. Circular sections A and B comprise an 80 mm radius and an insulation air gap of 33 mm [41].

microscopic surface irregularities), which generate optical errors distorting the reflected image. To reduce the impact of lateral shading, bypass diodes are employed, which allows the PV arrays to generate electricity at a lower capacity [32].

Solarus is the main and exclusive manufacturer of stationary low concentrating PVTs for commercial purposes [33]. The Solarus PowerCollector (PC) is a low concentrating PVT solar collector with an asymmetric CPC reflector geometry, which was designed to cope with the asymmetric solar radiation profile at high latitudes. Additionally, and due to the reflector design features (e.g. asymmetric geometry), the collector has a substantial gap between the reflector and the receiver (i.e. gap size is set by the receiver width), which leads to a larger shadow and therefore translated into a worse IAM profile. Hence, it is crucial to improve the reflector geometry into a symmetric geometry, to be able to cope with the more symmetric radiation profile at low and medium latitudes, and consequently an improved IAM profile. Therefore, the following study allows the comparison between a symmetric and an asymmetric geometry for PVT technologies. Two symmetric CPC geometries are suggested and compared with the asymmetric Maximum Reflector Collector (MaReCo) geometry of the Solarus PC.

The performance assessment emphasizes the main parameters that characterize a CPVT solar collector, such as, the electrical and thermal IAM (i.e. transversal and longitudinal), electrical peak performance, heat loss coefficient and overall optical efficiency. The evaluation of the proposed CPC reflector geometries will allow the reader to draw specific conclusions and an accurate performance comparison with the Solarus PC. Therefore, the performance assessment aim is to increase both electrical and thermal efficiencies of a CPVT solar collector, while having a lower concentration factor, and thus a reduced overall cost.

Additionally, in the following Section 2, both symmetric and asymmetric CPC reflector geometries, as well as the solar collector material description are presented. Section 3 presents the solar collector testing procedure. The main optical performance models used to assess the main CPVT collector characteristics are presented in Section 4, and as a final point, the results and discussion are presented in Section 5. The main findings are summarized in Section 6.

2. CPC-PVT solar collector design and methods

2.1. CPC reflector design

The general form of the design concept (presented in Fig. 2 under the designation of CPC 2) was based on an ideal CPC geometry, which is composed of a circular and parabola sections with their optical axis defining the accepted radiation interval.

For both geometries, the reflector section is divided into four main sections A, B, C and D. Section C has it focal point on the right edge of the receiver, whereas section D (which comprises a parabolic arc above absorber line) has a focal point on the top left edge of the receiver. The main difference between CPC 2 and CPC 1 lies in the 24 mm gap in section A (Fig. 3).

The reflector material has been provided by Almeco (Solar Vega SP295f) with a spectral reflectivity in the visible range of $\rho = 95\%$, a specular reflectance of $\geq 91\%$ and a total solar reflectance of 92%. The

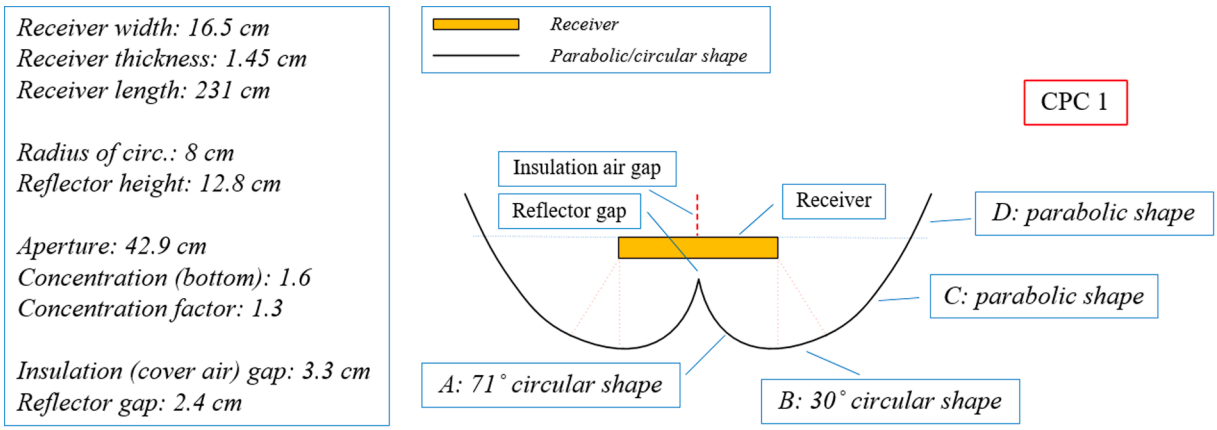

Fig. 3. CPC 1 geometry cross-section view, which comprises a 71° circular section A, a 30° circular section B and a parabola section C/D with the same centre point and radius. An insulation air gap of 33 mm and a gap between the bottom middle receiver side and circular intersections (section A) of 24 mm are also schematized [41]. Theoretical acceptance-half angle of 30°.

Table 1
Summary of the main parameters for each geometry design concept.

Geometry	Concentration factor (C_i)	Reflector length [mm]	Reflector depth [mm]	Air gap[1] [mm]	Gap[2] [mm]	Radius[3] [mm]	Theoretical acceptance half-angle (θ_c) [°]	Circular section arc-angles [°]
CPC 1	1.3	2350	128	33	24	80	30	101°
CPC 2					–			120°

[1] Distance between top receiver side and glass cover.
[2] Distance between the bottom receiver side and the mid reflector (section A).
[3] In order to fit both circular sections A and B with the same radius of 80 mm, the centre point of these arc-circumferences was set to 2.5 mm and 6.2 mm from the bottom edge of the receiver for CPC 2 and 1, respectively.

receiver has a length of around 2350 mm. An insulation air gap of 33 mm between the receiver and the glass cover has been set on both CPC geometries to reduce convection losses. Table 1 presents a more detailed assessment of the main parameters of each geometry.

In order to fit both circular sections A and B with the same radius of 80 mm, the center point of these arc-circumferences was set to 2.5 mm and 6.2 mm from the bottom edge of the receiver for CPC 2 and 1, respectively. This margin was set to cope with the edge of the PV cells, which will increase the light collection onto the PV cells.

2.2. Solarus powercollector reflector geometry

The aim is to introduce a refined CPC geometry for a PVT technology that can outperform the Solarus PC (Fig. 4), which is based on the asymmetric roof-integrated Maximum Reflector Concentration (MaReCo) geometry presented in [34]. The collector has been designed with an overall concentration factor of 1.5 and a bifacial absorber placed under the glass cover. All the incoming radiation up to the normal of the cover glass is accepted as the design concept has an optical axis of 90° from the cover glass.

The solar irradiation at low solar altitudes during winter is typically very low, which leads to a relatively narrow annual irradiation distribution in the north south plane, meaning that a CPC solar collector with a small acceptance angle can be designed. This principle has been employed while designing the asymmetric MaReCo reflector design which has a small acceptance angle, a long bottom edge reflector for summer irradiation and a short over edge reflector for winter irradiation. The Solarus PC has no over edge reflector, thus it is not optimized for lower latitudes where the radiation is high throughout the year. Moreover, an improved reflector geometry is imperative to increase the market share of concentrating PVT solar collectors.

2.3. Collector materials and bifacial PVT description

Both design concepts, as well as the PC use the same bifacial PVT absorber design with identical PV cell technology and dimensions. The bifacial PVT receiver has a receiver core with 2310 mm of length, a width of 165 mm and a thickness of 14.5 mm (Fig. 5).

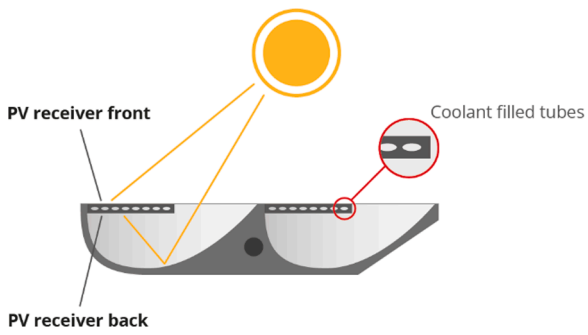

Fig. 4. General cross-section view of the PC collector with a MaReCo geometry (optical axis of 90° from the cover glass).

Fig. 5. CPVT collector comprising two geometries (CPC 1 and 2) with identical PVT receivers (PV cell string configuration of 8-11-11-8 PV cells).

The cell string layout has a total length of 2100 mm which comprises 38 one-third-size PV cells to lower the amount of current in each cell, which is divided into four sub-strings (8–11-11–8 PV cells), each one with one diode. The PV cells are encapsulated in a silicone gel from Wacker (Elastosil Solar 2205) with a total thickness of 3.5 mm (Fig. 6), with a reported thermal conductivity of 0.2 W/m.K and a light transmittance of 97%.

The PVT absorber has eight elliptical channels to increase the heat transfer between the aluminium receiver core and the HTF, decreasing in this way the PV cell temperature and thereby enhancing the electrical efficiency. The selected PV cells from Lightway Solar are characterized by an electrical efficiency of 20.1% and the main cell characteristics are presented in Table 2.

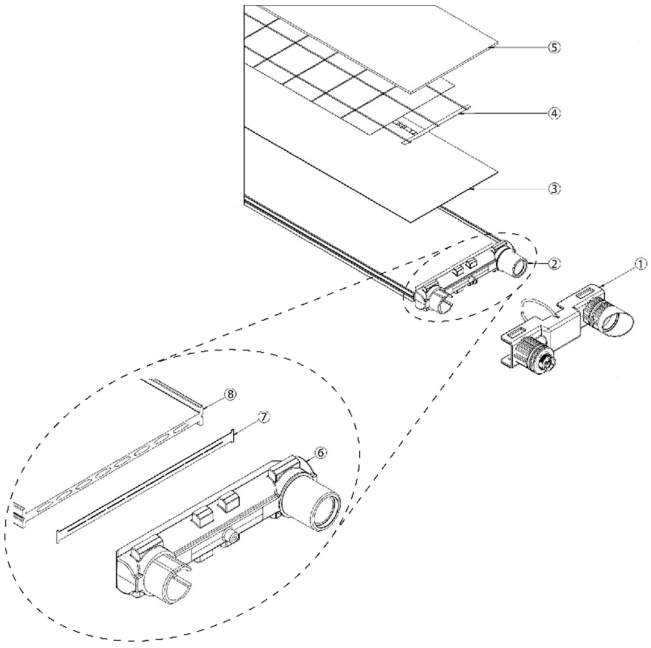

Fig. 6. Solarus bifacial PVT receiver: (1) receiver end cap; (2) PVT receiver; (3) 1st layer of Wacker-Elastosil Solar 2205; (4) monocrystalline PV cell string (8-11-11-8 connected in series); (5) 2nd layer of Wacker-Elastosil Solar 2205; (6) aluminium receiver end; (7) flow restrictor and (8) aluminium receiver core.

Table 2
Summary of the main parameters that characterize the one-third-cut PV cells.

Efficiency [%]	P_{mpp} [W]	V_{mpp} [V]	I_{mpp} [A]	V_{oc} [V]	I_{sc} [A]	Temperature coefficient [%/°C]
20.1	1.57	0.53	2.96	0.63	3.13	−0.37

The electrical power output of PV modules can be improved by employing smaller sized silicon solar cells as this can effectively reduce the series resistance loss due to lower cell-to-module losses [35]. Additionally, by having one-third-size PV cell, the theoretical maximum output power P_{mpp} and short-circuit current I_{sc} should be equal to one-third of the corresponding full-size cells, whereas the open-circuit voltage V_{oc} should remain the same.

Furthermore, a low-iron solar cover glass from Scheuten (SolarFloat Glass) and a Plexiglas Optical HT side gable protection with a thickness of 4 mm have been added to the collector design concept. The parameters that characterize both gable and solar glass are presented in Table 3.

It is important to note that the PVT receiver, the solar glass cover and the reflector material are the same materials as the ones used in the Solarus PC and have been donated by Solarus. This way the differences solely relate to the reflector geometry which will lead to more accurate results when comparing both geometry designs.

Moreover, the development of the newly CPC solar collector allowed a decrease of −15% in total gross area and −38% in the total solar collector height, which leads to a direct cost reduction (e.g. less material).

3. Standardized measurement of electrical and thermal performance

Stagnation temperatures in flat plate ST collectors often exceed 200 °C, therefore it is imperative that the solar collector materials/structure withstand these temperatures, especially in concentrator solar collectors. The stagnation temperatures in stationary low concentration PVT collectors are typically around 180 °C, as the CPVT Solarus PC [33]. The high stagnation temperatures of PVT collectors impose new challenges for the employed materials and components, as well as for the design and construction of PVT collectors. Two major causes for failure are observed in PVT solar collectors as a result of excessive temperatures: thermo-mechanical stress and exceeding of critical material temperatures [24]. Furthermore, apart from the challenges of high stagnation temperatures that stationary CPVT solar collector's come across, the focal line produced by the reflection of solar radiation into the PV cells increases the importance of specific and methodic material selection.

Moreover, the electrical performance of the CPVT collector has been characterized according to parameters presented in the standard IEC 62108 [36]. On the other hand, the thermal performance was characterized by a Steady-state (SS) testing method, which is described under the ISO 9806:2017 testing procedure guidelines. Furthermore, the standard ISO 9806:2017 for SS method states that concentrating collectors with transparent cover and with concentration ratio C_i lower than 3 suns are treated as flat-plate glazed collectors and that wind speed dependency can be neglected.

To accurately carry out these specific field testing procedures a new thermal test rig (Fig. 7) has been designed to cope with the specifications of the Solar Keymark standard. Additionally, an electrical measurement system to address the electrical parameters of any type of solar collectors have been updated.

The solar collector test facility is composed of a hydraulic and electric circuit designed for domestic ST and PV performance characterization. For both electrical and thermal performance characterization, several testing measurement equipment has been used, such as two KippZonen (CMP3 for diffuse and CMP6 for global radiation) pyranometers (installed in the same plane as the solar collector), IV tracer (in-house development), ambient and HTF temperature Pentronic-7420000 (Pt100) sensors, two Wilo-Stratos-Z flow pump, several Siemens electromechanical actuators SAS81 for valves, few pressure transmitters MBS 3000, a degasser SomaTherm-Reflex Servitec Mini and two Omega FMG70B electromagnetic flowmeters. Table 4 presents both the thermal and electrical measurement equipment accuracy.

The test setup apparatus consists of a solar collector closed loop and a domestic hot water open loop (presented in Fig. 8). Furthermore, the

Fig. 7. Thermal test rig design to cope with the specifications of ISO 9806:2017 testing procedure with an auxiliary pump station.

Table 4
Thermal and electrical measurement equipment and respective accuracy deviation accordingly to manufacturer datasheets.

Thermal measurement equipment	Value	Deviation
Flow rate $\dot{m}$ [kg/s.m^2]	0.009–0.2	±1.5%
Temperature interval ΔT [°C]	0–90	±0.04%
Pressure interval ΔP [Bar]	Up to 6	±1.5%
Heater [°C]	10–90	±0.04%
Pressure transmitter [Bar]	6	±1%
Electrical measurement equipment	*Data*	*Deviation*
Pyranometer CMP3 [W/m^2]	Up to 2000	±1.5%
Pyranometer CMP6 [W/m^2]	Up to 2000	±1%
IV Tracer [I] [V]	–	0.1%

Table 3
Summary of the main parameters that characterize the low iron solar glass and the Plexiglas side gable.

	Emissivity [%]	Thickness [mm]	Thermal conductivity [W/m.K]	Transmittance[1] [%]
Cover, Solar glass[2]	84	4	1	91 [+/−0.5]
Gable, Plexiglas[3]	94	4	0.18	92 [+/−1]

[1] Reference to ISO 9050. Restricted to wavelengths from 0.3 to 1.2 μm.
[2] Reference to Scheuten SolarFloat Glass at https://www.scheuten.com.
[3] Reference to Plexiglas Optical HT at https://www.plexiglas.de/en/products/plexiglas/plexiglas-optical.

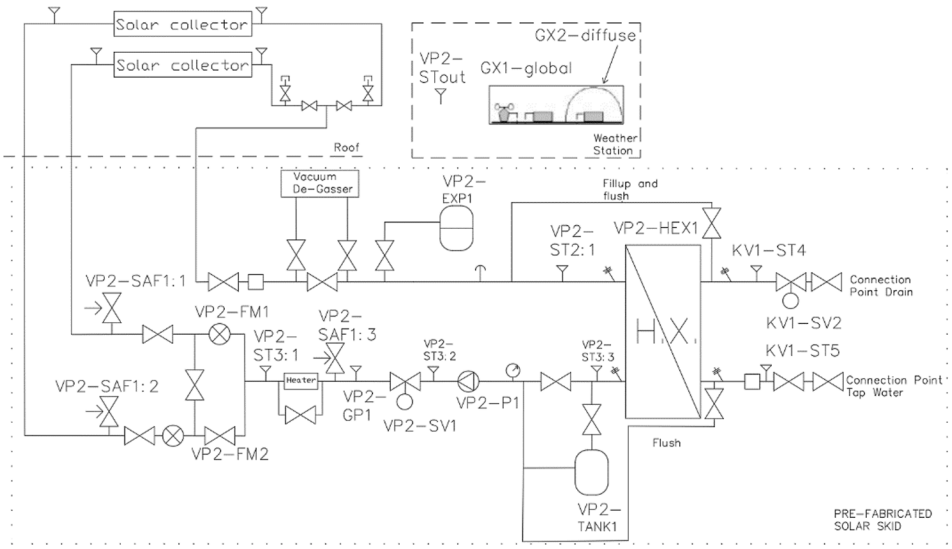

Fig. 8. Technical drawing of the hydraulic rig composed of several temperature and pressure sensors, a heat exchanger, a vacuum degasser, expansion vessel, mixing tank (for a more homogeneous temperature), as well as a heater for constant inlet temperature.

solar collector loop relates to the HTF flowing between the collector and heat exchanger, supplied by a fixed flow rate. A mixture of 20% ethylene glycol (with a heat capacity of 2200 J/Kg.K) and 80% of pure water is used as HTF with an overall heat capacity of 3813 J/Kg.K.

The closed-loop is composed of the following components:

- Programmable logic controller: All regulation and control are done by an Abelko Webmaster Pro/Ultrabase PLC system, which allows for remote control of the system.
- Automated flow control: The flow is controlled through a proportional-integral-derivative (PID) regulator and a frequency-controlled pump, which allows the user to set the desired flow rate and automatically adjust to any pressure drop.
- Collector inlet temperature control: Incoming hot water from the solar collectors is first cooled by tap water (through a heat exchanger) to a temperature slightly below the desired collector inlet temperature. The water is stored in a 10 L storage tank for buffering and then heated to the desired temperature with a 4.5 kW heater from RELEK Produktion AB.
- Temperature measurement/thermal performance characterization: PT100s are used to measure the inlet and outlet temperatures of thermal collectors, as well as ambient temperature. The inlet and outlet temperature sensors have been installed against the flow, thus creating turbulence within the pipe, and therefore yield more accurate measurements [37].
- Vacuum degasser: For accurate measurement and results, the circuit must be completely free of air. Therefore, a degasser has been installed as it allows the flow to go through a chamber of lower pressure where air bubbles increase in size and are subsequently removed. Water that is free of air will naturally absorb any incoming air from the circuit and therefore the system eventually will be completely air-free (theoretically), even in places where the flow is too low to physically move trapped air bubbles.
- Insulated stainless steel piping: All piping in the test rig is made out of stainless steel pipes which decreases the pressure drop and reduces significantly the possibility of corrosion [38].

Table 5 shows the test condition limits for the SS methods presented in ISO 9806:2017 and the deviation from the performed outdoor testing.

In order to a lower difference between T_{out} and T_{in} the standard for ST collectors ISO 9806–2017 has been adapted and therefore the mass flow rate $\dot{m}$ has been set to 0.03 kg/s.m^2.

The testing equipment is connected to a CR1000 datalogger from Campbell Scientific that monitors, records and processes the data with time-step measurements of 30 sec. All the measurements were then treated as 10-minute average data to compress and increase data accuracy. Moreover, the following Fig. 9 presents a flow chart of the employed methodology for this manuscript development.

Table 5
Test conditions and maximum allowed deviation for the Steady-State method, according to the international standard for ST collectors ISO 9806-2017 for thermal measurements. For electrical measurements, the test conditions and maximum allowed deviations are presented according to the IEC 62108:2017 standard.

	Steady-state method ISO 9806:2017			IEC 62108:2007	
	Required value	Allowed deviation	Measured values during testing	Required value	Allowed deviation
Global radiation, G_{global} [W/m^2]	>700	±50	>900 ± 40	>700	<2%
Incidence angle, θ_i [°]	<20	–	<7	–	–
Diffuse radiation, $G_{diffuse}/G$ [%]	<30	–	<14	–	–
Mass flow rate, $\dot{m}$ [kg/s.m^2]	0.02	±1%	0.03	–	–
Inlet temperature, t_{in} [K]	–	±0.1	±0.1	–	<1 °C per 5 min.
Ambient temperature, t_a [K]	–	±1.5	±1.5	–	<2 °C per min.

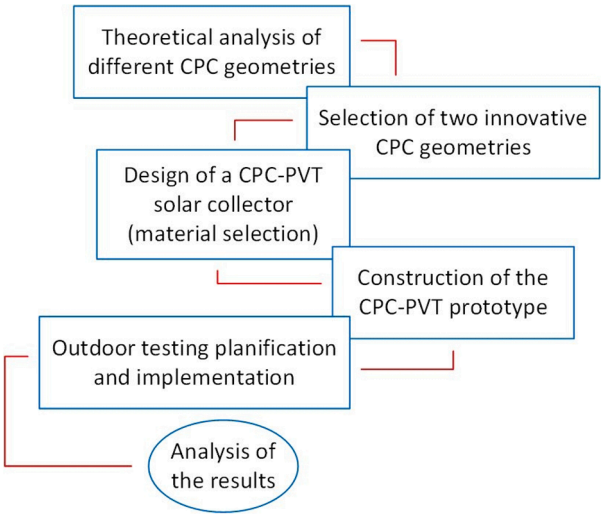

Fig. 9. Flow chart diagram of the implemented methodology.

3.1. Electrical and thermal performance method procedure

For both thermal and electrical performance testing procedures, the hybrid CPVT solar collector has been east-west oriented, with different collector tilts set by (90 - θ_{NS})° for a given day. This tilt was adjusted to ensure that the incidence angle was optimal for Gävle (Sweden: 60.7 °N, 17.1 °E) at midday, as can be seen in Fig. 10.

For an optimal measurement of both transversal and longitudinal IAM, the measurements should be performed around the equinox. During the equinox (21st of September and March), the south projection angle is fairly constant, as can be seen in Fig. 11, which does not require azimuth and tilt adjustments, and thus no correction factors needed. Therefore, the presented work employed the measurements for each

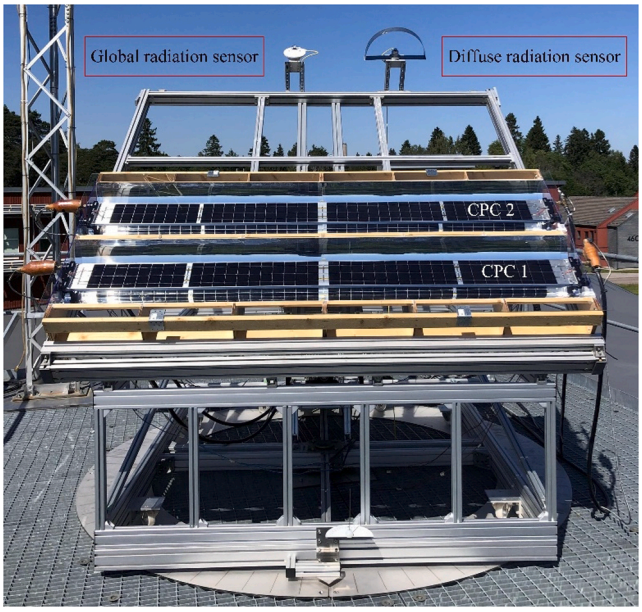

Fig. 10. CPVT solar collector test apparatus (orientation: east-west direction) for different testing procedures with both pyranometers for global (KippZonen CMP6) and diffuse (KippZonen CMP3) radiation measurement.

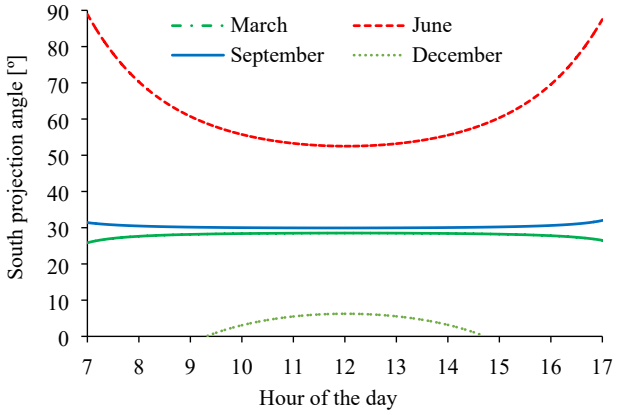

Fig. 11. South projected angle for the equinoxes and solstices (summer and winter). Location: Gävle, Sweden.

IAM during the equinoxes.

To perform measurements on electrical $IAM_{Long.}$ (longitudinal direction), the collector has been east-west oriented, where the angle between the collector and the sun in the transversal direction angle is 0°, which decreases the need for any correction factors, as the projected solar altitude will have a profile movement in an east-west plane.

On the other hand, for the transversal electrical IAM, the previously described $IAM_{Long.}$ procedure has been replicated, however, the collector has been placed in a north-south position (rotated 90° from the initial position), so that the longitudinal direction angle is 0°.

4. Optical efficiency

4.1. Optical design concepts

CPC concentrators are non-imaging concentrators that do not require a tracking system due to their ability to reflect all available incident radiation, both beam and diffuse, into a receiver over a wide range of incidence angles. The boundary limits of these incidence angles are defined as the acceptance angle of a concentrator, where all the incoming incident radiation, both beam and diffuse, that falls within this acceptance angle will be reflected into the receiver. A wide range of acceptance angles increases the attractiveness from the point of view of system simplicity, flexibility and cost-effectiveness of CPC reflector geometries.

It combines two parabolic reflectors, either symmetric or asymmetric, on each side. Each side of the parabola has its focus length at the lower edge of the other parabola (Fig. 12). The distance from one end of the receiver to the focal point is given by the point where the parabola will reflect the incoming sunlight when the angle of incidence is lower or equivalent to the acceptance angle. The angle between the axis of the collector and the line connecting the focus of one of the parabolas with the opposite edge of the aperture is called acceptance half-angle θ_c. This angle is characterized by the maximum angle at which the incoming sunlight can be captured by the solar concentrator.

An ideal CPC is characterized by parallel surfaces at the upper-end points of both parabolas, which do not contribute meaningfully towards a higher radiation collection, therefore, a CPC reflector geometry can be truncated without compromising the overall performance.

Truncation is applied to increase optical efficiencies (i.e., decreasing the average number of reflections) and energy yields. On the other hand, this leads to higher heat losses per aperture area and thus lowers the

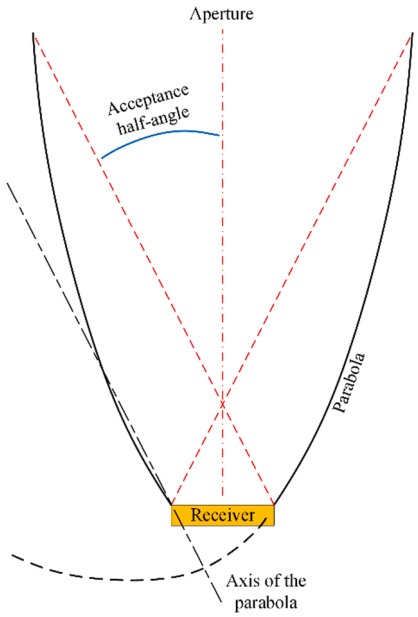

Fig. 12. Cross-section of a symmetrical non-truncated CPC.

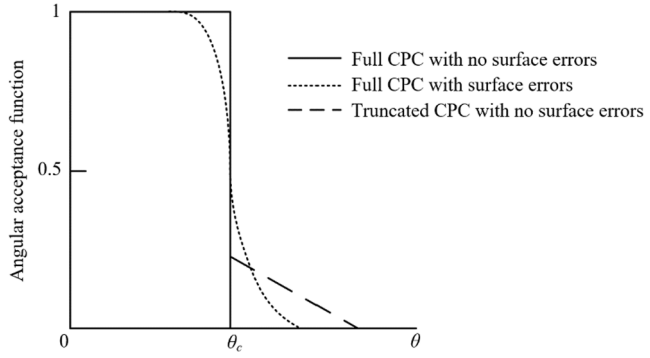

Fig. 13. Acceptance angle function for a full (with and without surface errors) and truncated (with no surface errors) CPC.

amount of unnecessary shading [39,34]. Moreover, limited truncation does not affect the acceptance half-angle, in contrast to the significant changes in concentration and height-to-aperture ratio, as well as in the average number of reflections [40]. Fig. 13 presents the theoretical fraction of incident radiation (i.e. the angular acceptance function) for a given aperture at an angle θ that hits the absorber as a function of θ.

Other useful expressions that describe the design of CPC concentrators are shown in Eq. (1) and (2). The following equations relate the focal length of the side parabola to the acceptance half-angle (θ_c), receiver size (2a '), and height of the collector (h), being f the focal length.

$$f = a'(1 + \sin\theta_c) \tag{1}$$

$$h = \frac{f \cdot \cos\theta_c}{\sin^2\theta_c} \tag{2}$$

These types of concentrators are built for each ray with an angle θ that comes into the CPC aperture with an angle smaller than θ_c to be reflected into the receiver. The ray will be reflected to the atmosphere if the angle θ is greater than θ_c.

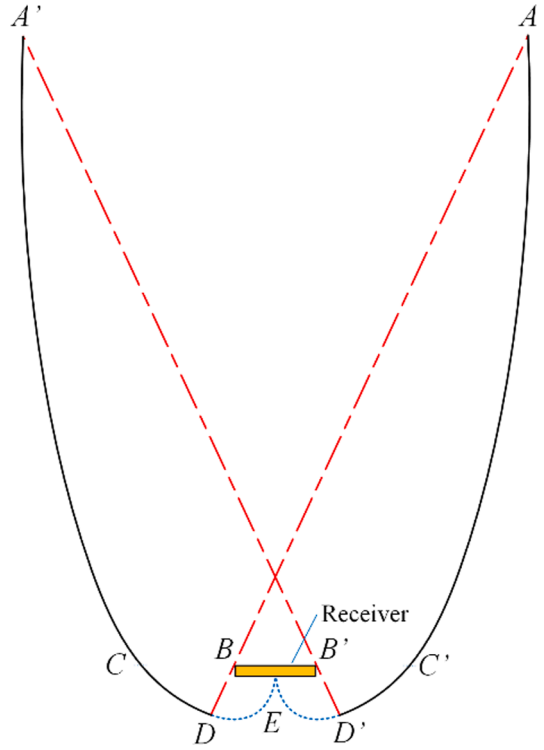

Fig. 14. Ideal concentrator design for a transverse fin absorber.

An ideal concentrator design for a transverse fin absorber (horizontal) can be found and has been presented by Rabl (1976a) and schematized in the following Fig. 14.

- Section ED' and ED receive reflected illumination, which are involutes of sections EB' and EB, respectively;
- ED' is an arc-circle with centre in B'. $D'C'$ is a parabola with focus in B' and axis $D'A'$. $C'A$ is a parabola with focus in B and an axis parallel to $D'A'$;
- $C'A$ and CA' have their focus on B and B', respectively;
- $C'D'$ and CD have their focus on B' and B, respectively.

Therefore, two reflector geometry concepts based on a CPC geometry have been coupled with a bifacial PVT receiver. Firstly, a CPC reflector geometry concept has been adjusted and truncated. Secondly, a CPC reflector geometry with a gap between the horizontal PVT receiver (comprising cooling fluid channels inside the aluminum core of a PVT absorber) and the reflector geometry is presented. Both design concepts are based on the reference work made by Cabral et al. [41], which was based in the developments of CPC solar collectors presented theoretically in Winston and Hinterberger [40,42,43], Collares-Pereira et al. [44], Rabl et al. [45], and Carvalho et al. [39].

4.2. Theoretical optical efficiency

Optical efficiency is a key element to the electrical and thermal performance characterization of a CPVT collector, as the system efficiency is set by the optical properties of the cover glazing (transmittance, τ), the reflector material (effective reflectance ρ, which includes the number of bounces) and the PV solar cell (absorptance, α). In this specific case, the cell absorptance is negligible, as it is the same for a reference system without concentrators and glazing. Eq. (3) describes the theoretical optical efficiency for electricity production for

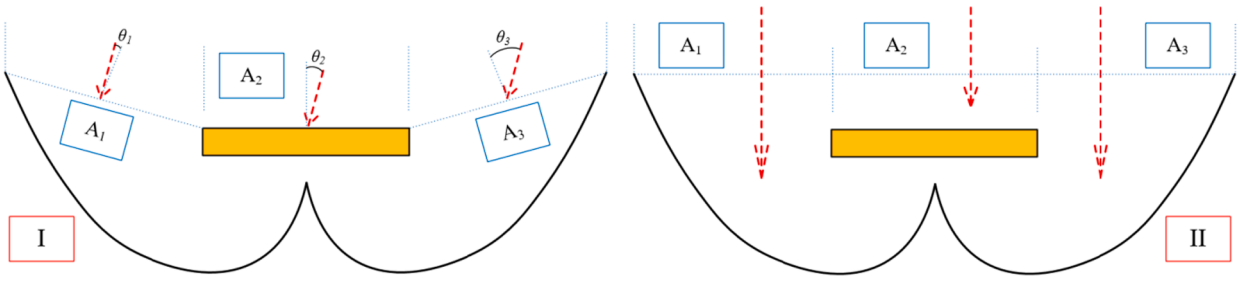

Fig. 15. I: Theoretical optical efficiency (I) for electricity production for all angles of incidence. II: Theoretical optical efficiency for electricity production at normal incidence.

any angle of incidence (i.e. in which $A_{reflector\_x}$ and A_{cell} are 136 and 165 mm, respectively).

$$\eta_{opt} = \frac{\tau \cdot \left(G_{beam} \cdot \cos\theta_1 \cdot A_{reflector\_1} \cdot \rho + G_{global} \cdot \cos\theta_2 \cdot A_{cell} + G_{beam} \cdot \cos\theta_3 \cdot A_{reflector\_3} \cdot \rho + 2 \cdot G_{diffuse} \cdot \frac{A_{reflector\_4}}{Cbottom} \right)}{A_{aperture} \cdot G_{global}} \quad (3)$$

θ_1 corresponds to the angle of incidence with the normal of $A_{reflector\_1}$ (i.e. distance between receiver and reflector top left edges). Additionally, θ_2 corresponds to the angle of incidence with the A_{cell} normal. Following the same thought, θ_3 corresponds to the angle of incidence with the normal of $A_{reflector\_3}$ (i.e. distance between receiver and reflector top right edges). $A_{reflector\_4} = A_{reflector\_1} + A_{reflector\_3}$. Moreover, from the principles applied in Eq. (3), it is possible to derive the theoretical optical efficiency for electricity production at normal incidence (i.e. under the acceptance angle, in which $A_{reflector}$ corresponds to 132 mm (i.e. $A_{reflector} = (A_{aperture} - A_{cell})/2$) and A_{cell} to 165 mm) by applying Eq. (4).

$$\eta_{opt} = \frac{\tau \cdot \left(2 \cdot G_{beam} \cdot A_{reflector} \cdot \rho + G_{global} \cdot A_{cell} + 2 \cdot G_{diffuse} \cdot \frac{A_{reflector}}{Cbottom} \right)}{A_{aperture} \cdot G_{global}} \quad (4)$$

The theoretical optical efficiency for electricity production presented by Brogen et al. [46] takes into account only the beam radiation fraction on both $A_{reflector}$ (i.e. $A_{reflector} = A_{aperture} - A_{cell}$ at normal incidence) and A_{cell} (i.e. front area of the PV cell), therefore, both Eq. (3) and Eq. (4) have been refined and updated to consider the individual influence of the beam and global radiation in $A_{reflector}$ and A_{cell}, respectively. A schematic representation of how Eq. 3 and 4 have been developed is presented in the following Fig. 15.

4.3. Optical efficiency from I_{sc} measurements

As the short-circuit current I_{sc} of a photovoltaic module is proportional to the irradiance, at a constant temperature, the optical efficiency can thus be calculated from the I_{sc} with corrections for the geometrical concentration ratio C_i, and measured global irradiated intensity G. Eq. (5) presents the correction factors for obtaining the optical efficiency of the reflector (including the glazing) from I_{sc} measurements [46].

$$\eta_{opt} = \frac{I_{sc,measured}}{I_{sc,standard\ module}} \cdot \frac{G_{STC}}{C_i \cdot G_{global}} \quad (5)$$

4.4. Optical efficiency from thermal measurements

The instantaneous collector output power Q (Eq. 6) can be obtained by measuring the solar radiation, flow rate and HTF temperature [47].

$$Q = \rho \cdot V \cdot c_p \cdot \Delta T / A_c \quad (6)$$

To describe the collector output power P, a simplified model has been applied, in which solar radiation, peak collector efficiency η_0 and the HTF temperature difference is used as input, as can be seen in the following Eq. (7) and simplified in Eq. (10) to access the heat loss coefficient U_1 and the optical efficiency from thermal measurements.

$$P = \eta_0 \cdot G - U1 \cdot \Delta T \quad (7)$$

Where,

$$\Delta T = T_m - T_a \quad (8)$$

$$T_m = \frac{T_{out} + T_{in}}{2} \quad (9)$$

From Eq. (9) is then possible to derive the collector efficiency by employing Eq. (10).

$$\eta = \eta_0 - c_1 \cdot \frac{\Delta T}{G} - c_2 \cdot \frac{\Delta T^2}{G} \quad (10)$$

5. Result and discussion

The following section presents different sets of results, such as electrical instantaneous peak power, optical efficiency from I_{sc} and thermal measurements, day and dark heat losses, and both transversal and longitudinal electrical/thermal IAM profile diagrams.

This paper aims at improving the reflector geometry of the Solarus PC while having few raw materials, a lower concentration factor and a wider acceptance angle. A more detailed assessment of the different tested results is presented in Appendix A (Table 15 and 16).

5.1. Daily electrical power

A clear sky day in June has been selected to provide a better understanding of the daily electrical performance profile of the LCPVT solar collector for both CPC 1 and 2 receiver sides (bottom and top). The data has been collected for the whole day of the 25th of June for a collector tilt of 38° and a constant HTF temperature of 24 °C is presented in the following Fig. 16.

The ambient temperature reached 32 °C. As expected, the CPC 1 top receiver side presents a typical pattern for a flat PV module, as it follows the solar radiation pattern reaching an electrical peak power of 48 W,

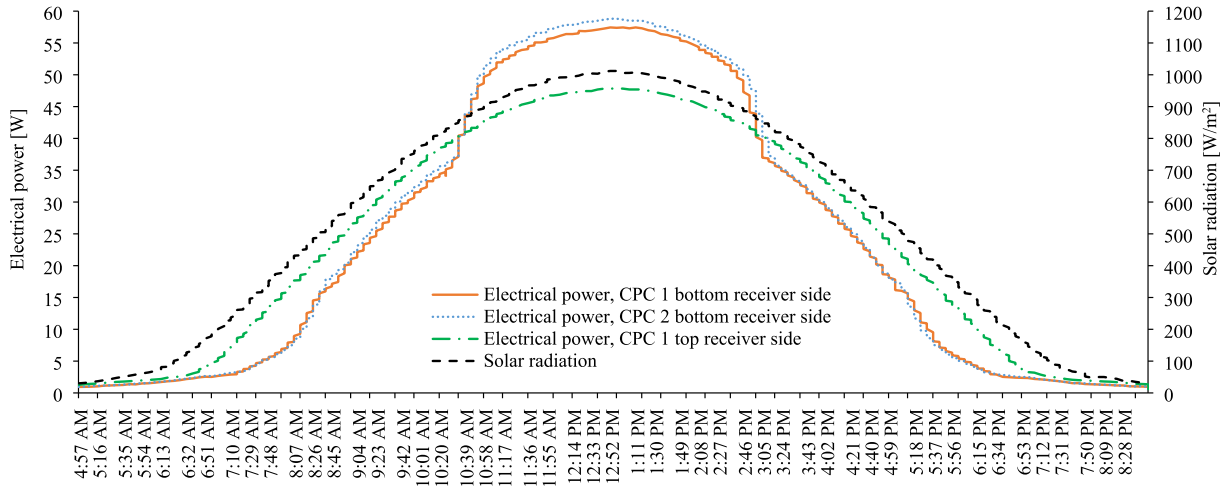

Fig. 16. Electrical power registered for the bottom receiver side of CPC 1 and 2, and top receiver side for CPC 1 in a clear sky day on the 25th of June.

which is in line, within the same magnitude, as the CPC 2 top receiver side electrical performance power (therefore, not plotted in Fig. 16 for simplicity). The bottom receiver side from CPC 2 showed a slight increment of around +1.7% when compared to CPC 1.

Furthermore, the pattern for both bottom receiver sides follow the solar radiation profile until 10:30 am and after 3 pm, which is explained by the bypass diode operation, which will bypass one sub-string. From 10:30 am to 3 pm, which comprises roughly one-quarter of the total measured electrical power, the PVT system is able to operate at its maximum power as the diode is no longer operating (since no significant side shading is registered), thus increasing significantly the electrical peak power during mid-day. This phenomenon can be seen by analysing the $V_{mpp.}$ of the bottom receiver side where an increment of 6 V was registered from 15 V up to 21 V (time: 10:30 am) and a decrease within the same voltage magnitude (time: 3 pm).

5.2. Electrical peak efficiency

By using active cooling and an improved reflector geometry the performance of the PV cells is expected to improve, thus increasing the electrical peak efficiency. Therefore, Fig. 17 shows the electrical peak efficiency diagram as a function of the module temperature for both CPC 1 and 2, where the influence of the HTF, solar radiation and PV cell temperature in the electrical peak efficiency is registered.

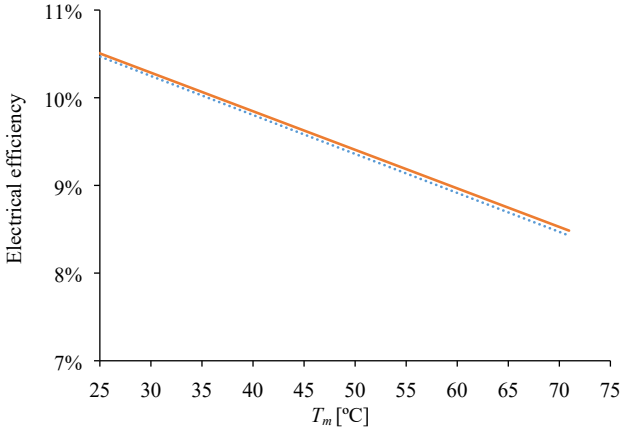

Fig. 17. Electrical efficiency per gross area of CPC 1 (solid orange line) and CPC 2 (dashed blue line). (For interpretation of the references to colour in this figure legend, the reader is referred to the web version of this article.)

An electrical peak efficiency of 10.6% (R^2 = 0.999) has been achieved for both CPC 1 and 2, for a module temperature of 25 °C. Fig. 17 also presents a steady electrical peak efficiency for higher temperatures, which can be translated into a temperature dependence coefficient of around 0.47%/°C. Additionally, the temperature has been monitored at the HTF level, which is lower than the PV cell temperature.

The electrical peak efficiency of CPC 1 and 2 showed an improvement of around $+16.6\%_{CPC1}$ and $+16.2\%_{CPC2}$ when compared with the Solarus PC.

After assembly, it is expected that the overall solar collector efficiency drops below the theoretical peak efficiency of a unique solar cell. This phenomenon can be explained due to reflection and absorption losses, as well as, manufacturing tolerances (distance between cells) that lead to non-producing "dead" areas. Furthermore, the connections between cells introduce resistance losses and although all the cells are theoretically batched together into power bands, the cells are not

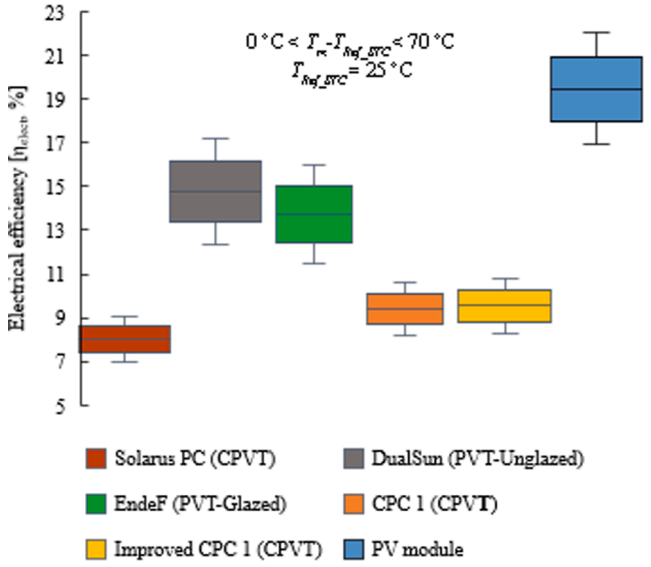

Fig. 18. Comparison of the electrical efficiency of an arbitrary flat-unglazed (e.g. DualSun), flat-glazed (e.g. EndeF) and low-concentrating (e.g. both Solarus PC and CPC 1 reflector geometry developed in this manuscript) PVT collectors, and a PV module. Efficiency is related to the gross area. The size of the coloured squares shows the lower and higher electrical efficiency range, which corresponds to the higher and lower temperature, respectively.

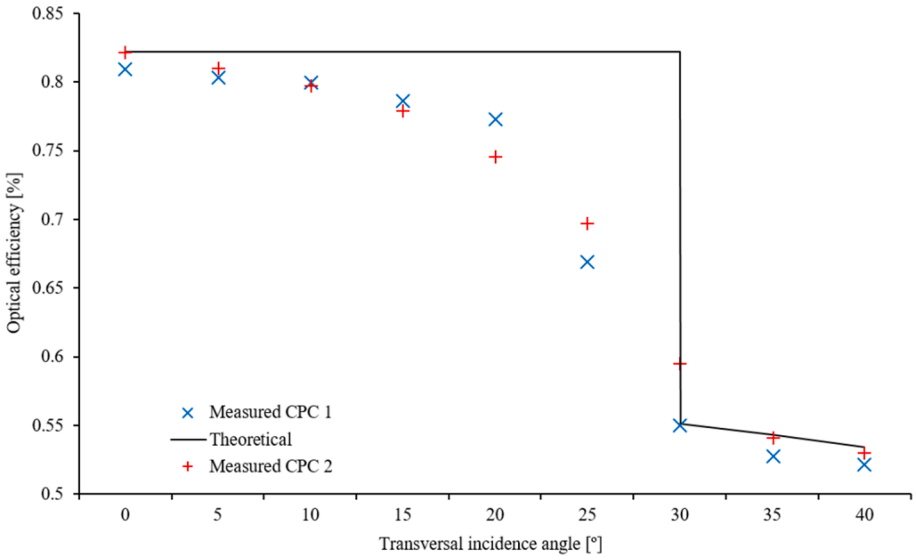

Fig. 19. Measured and theoretical optical efficiency as a function of transverse incidence angle calculated from measured I_{sc} current, for both CPC 1 and 2.

perfectly matched and therefore the electrical peak performance of a cell string connected in series will be set by the lowest-performing cell.

By employing the following Eq. (11), it is possible to address the electrical efficiency of different PVT technologies available in the market by taking into account the temperature coefficient of electrical power β, the standard panel efficiency $\eta_{el,STC}$, and the corresponding HTF mean fluid temperature t_m (presented in Eq. 9) and ambient temperature t_a [5].

$$\eta_{el\_col} = \eta_{el,STC} \cdot [1 - \beta \cdot (T_m - T_a)] \quad (11)$$

Therefore, a comprehensive theoretical comparison based on Eq. (8) between several PVT technologies brands (e.g. DualSun, EndeF and Solarus PC) and the low concentrating CPC 1 (i.e. solar collector developed in this manuscript) has been performed and presented in Fig. 18.

5.3. Optical efficiency from I_{sc} measurements

From the IAM testing procedure, the I_{sc} has been retrieved and the optical efficiency has been calculated, as the irradiance on the PV cells is proportional to the I_{sc}. From Eq. (3 and 4) the theoretical optical efficiency has been calculated as a function of the transverse incidence angles from 0° (normal incidence) up to 40°. Fig. 19 presents the results from the measured (i.e. derived from Eq. 5) and theoretical optical efficiency for the given transversal angle of incidence, which gives a theoretical optical efficiencies of 82% at normal incidence.

Typically, the measured efficiency decreases with the increment of the incident angles. Up to the theoretical acceptance-angle, which is comprised at 30° (where an abrupt decrease in efficiency is registered), the measured optical efficiencies have a fairly slow decrease in relation to the theoretical optical efficiency pattern. For incident angles higher than the theoretical acceptance angle the difference increases due to reflector imperfections (i.e. manufacturing problems and material

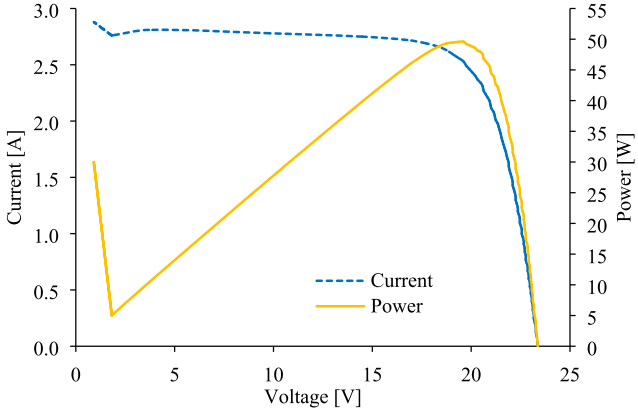

Fig. 21. IV curve at normal incidence (0° with normal of the solar collector) for the top receiver side at 1015 W/m^2.

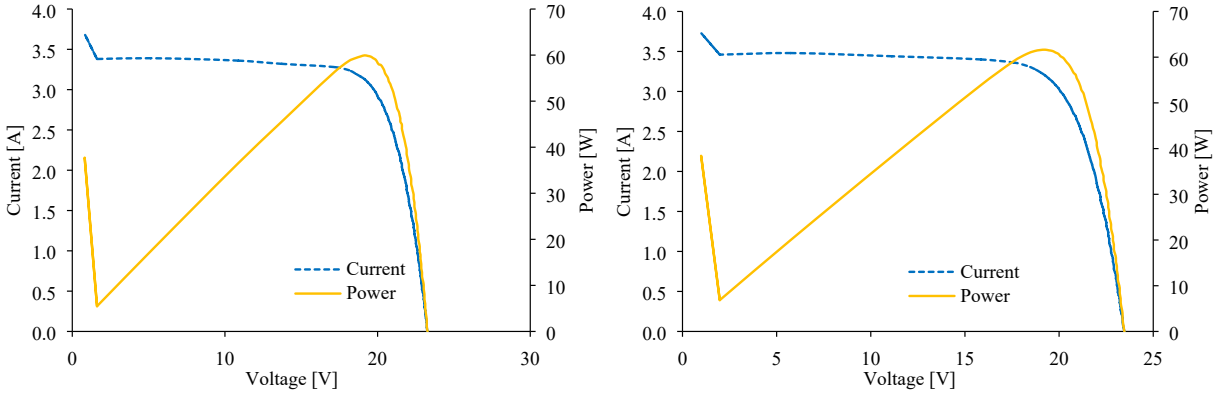

Fig. 20. IV curve at normal incidence (0° with normal of the solar collector) for the bottom receiver side of geometry CPC 1 (left image) and CPC 2 (right image) at 1015 W/m^2.

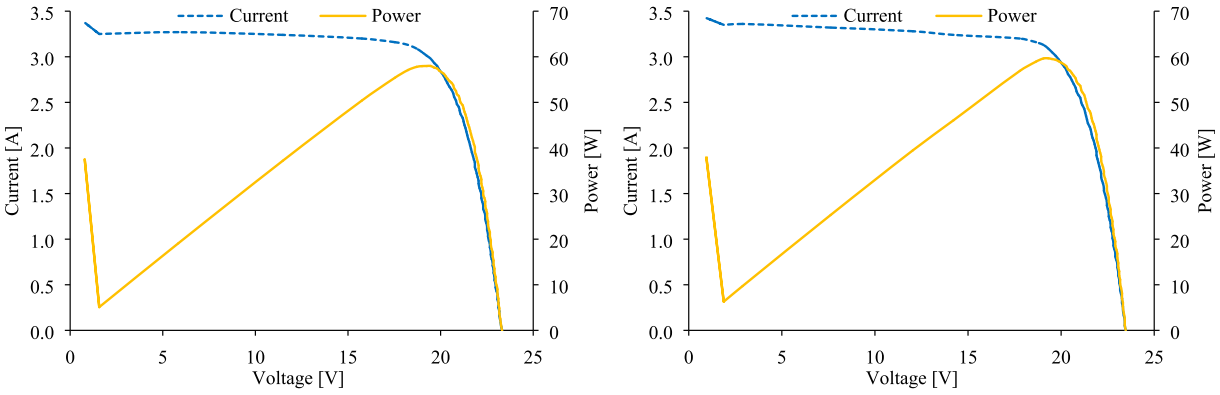

Fig. 22. IV curve at 5° from normal incidence (transversal direction) for the bottom receiver side of geometry CPC 1 (left image) and CPC 2 (right image) at 1000 W/m^2.

scattering) and therefore imprecise reflections. Furthermore, in view of fact that for different incidence angles the focal line shifts transversely the PVT receiver, the series resistance will vary as the edge busbar tend to carry most of the generated electric current. Moreover, the steep decrease between 20° and 30° for CPC 1 might be explained by the gap of 24 mm in section A, which will allow a portion of the reflected rays to pass under the absorber, and therefore to lower the overall efficiency. Additionally, the thickness of the PVT receiver has an impact on the measured acceptance-angle, which led to a lower measured acceptance-angle.

The specific IV curves are presented at normal incidence for both bottom (Fig. 20) and top receiver side of geometry CPC 1 and 2.

CPC 1 and 2 reached a P_{mpp} of 60 and 62 W (bottom receiver side), respectively, while their I_{sc} reached 3.4 and 3.5 A, respectively.

On the other hand, the top receiver side has a similar profile and electrical outputs as presented in the following Fig. 21.

A P_{mpp} of around 50 W and an I_{sc} of around 2.8 A have been registered for the top receiver side of both geometries, as it is not dependent on the geometry. The following Fig. 22 presents the IV curve at 5° from normal incidence (transversal direction) for the bottom receiver side of geometry CPC 1 and 2.

A transversal angle of incidence of 5° leads to a P_{mpp} of 58 and 60 W, and to an I_{sc} of 3.3 and 3.4 A for both CPC 1 and 2, respectively. The following Fig. 23 presents the IV curve at 10° from normal incidence

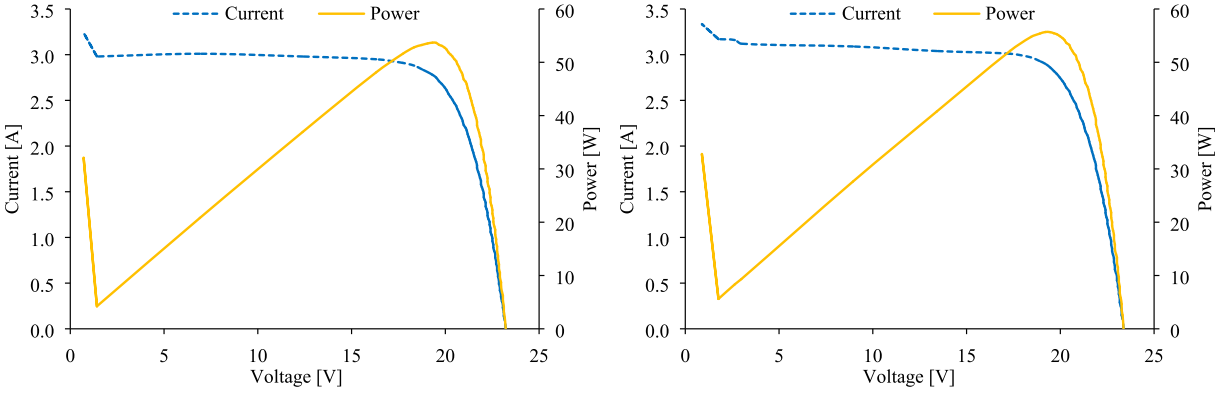

Fig. 23. IV curve at 10° from normal incidence (transversal direction) for the bottom receiver side of geometry CPC 1 (left image) and CPC 2 (right image) at 983 W/m^2.

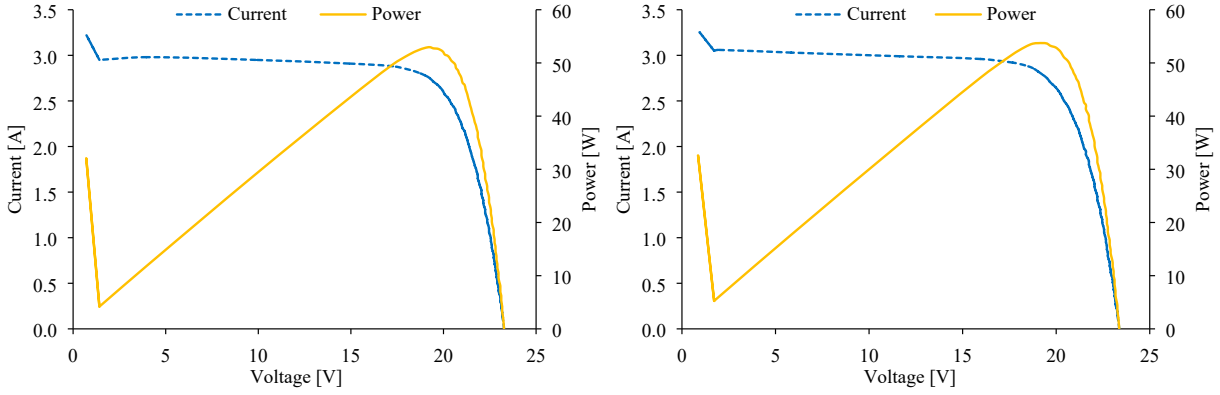

Fig. 24. IV curve at 15° from normal incidence (transversal direction) for the bottom receiver side of geometry CPC 1 (left image) and CPC 2 (right image) at 953 W/m^2.

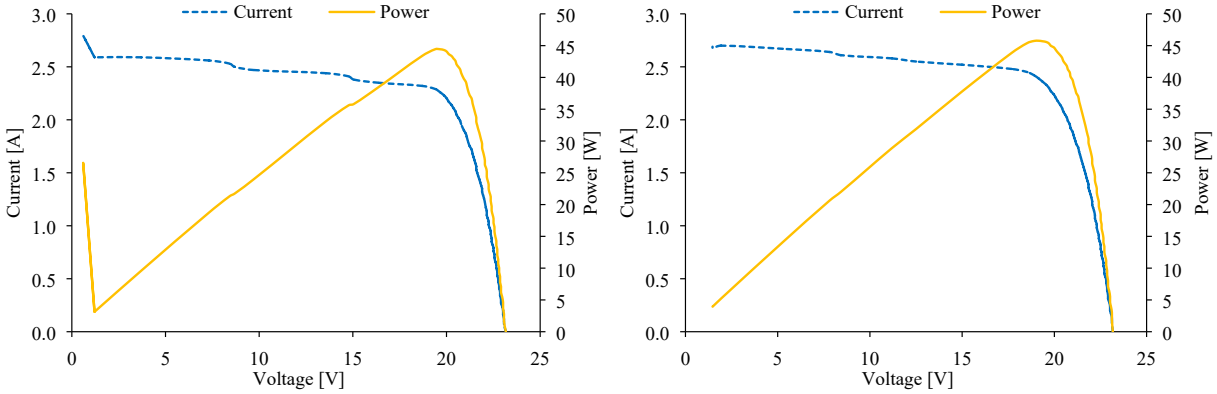

Fig. 25. IV curve at 20° from normal incidence (transversal direction) for the bottom receiver side of geometry CPC 1 (left image) and CPC 2 (right image) at 934 W/m^2.

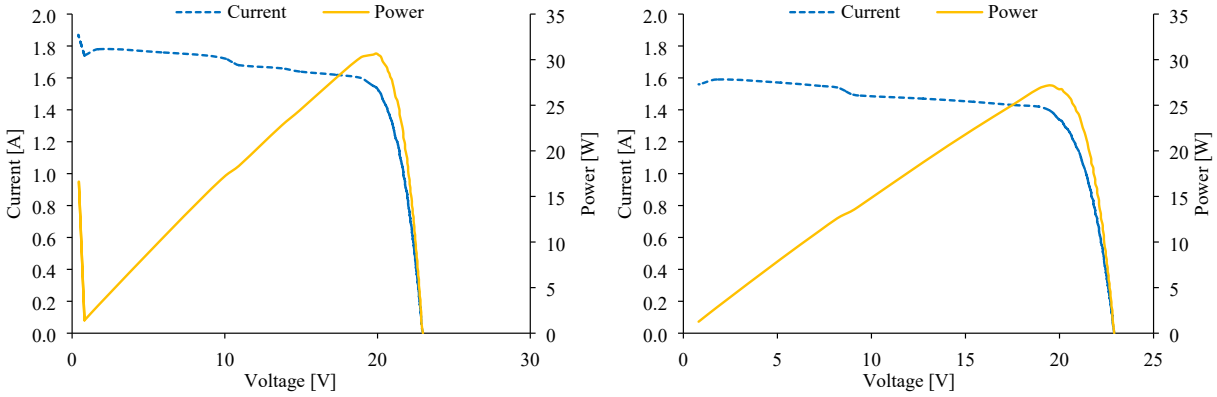

Fig. 26. IV curve at 25° from normal incidence (transversal direction) for the bottom receiver side of geometry CPC 1 (left image) and CPC 2 (right image) at 903 W/m^2.

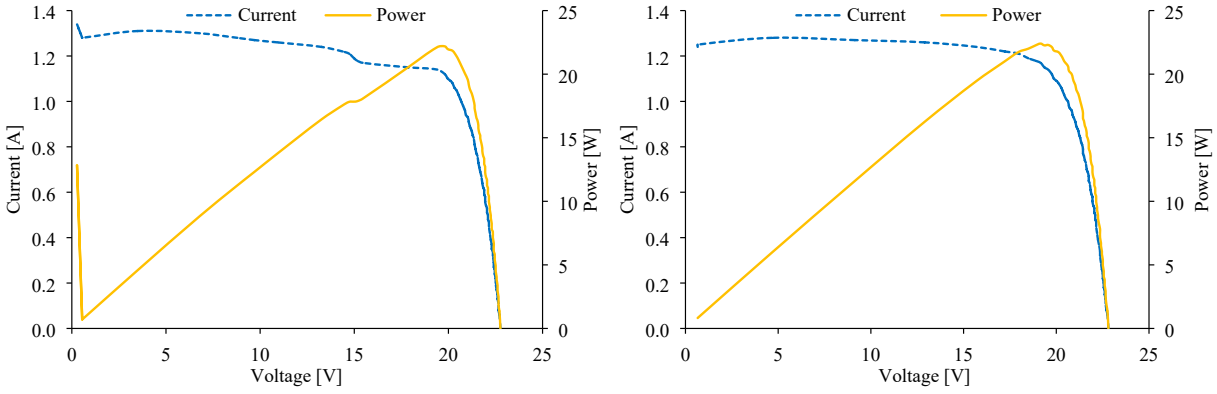

Fig. 27. IV curve at 30° from normal incidence (transversal direction) for the bottom receiver side of geometry CPC 1 (left image) and CPC 2 (right image) at 865 W/m^2.

(transversal direction) for the bottom receiver side of geometry CPC 1 and 2.

A transversal angle of incidence of 10° leads to a P_{mpp} of 54 and 56 W, and to an I_{sc} of around 3 and 3.1 A for both CPC 1 and 2, respectively. The following Fig. 24 presents the IV curve at 15° from normal incidence (transversal direction) for the bottom receiver side of geometry CPC 1 and 2.

A transversal angle of incidence of 15° leads to a P_{mpp} of 53 and 54 W, and to an I_{sc} of 3 A for both CPC 1 and 2, respectively. Additionally, Figs. 25 and 26 present the IV curve at 20° and 25°, respectively, from normal incidence (transversal direction) for the bottom receiver side, where it is possible to see the impact of the acceptance-angle in the PV cell string electrical performance.

A transversal angle of incidence of 20° leads to a P_{mpp} of 44 and 46 W, and to an I_{sc} of around 2.6 and 2.7 A for both CPC 1 and 2, respectively. The following Fig. 26 presents the IV curve at 25° from normal incidence (transversal direction) for the bottom receiver side of geometry CPC 1 and 2.

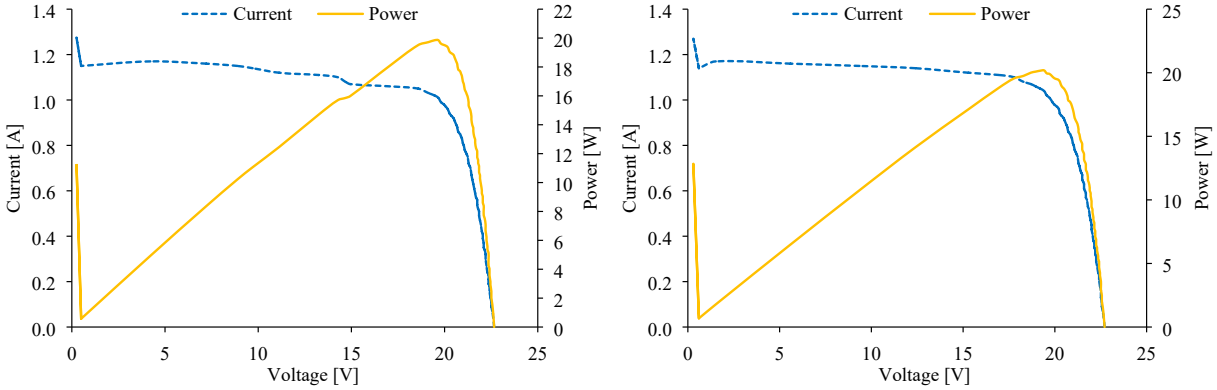

Fig. 28. IV curve at 35° from normal incidence (transversal direction) for the bottom receiver side of geometry CPC 1 (left image) and CPC 2 (right image) at 831 W/m^2.

At 25° from normal incidence (transversal direction), the P_{mpp} further decreases to 31 and 27 W, and to an I_{sc} of 1.8 and 1.6 A for both CPC 1 and 2, respectively. The following Fig. 27 presents the IV curve at 30° from normal incidence (transversal direction) for the bottom receiver side of geometry CPC 1 and 2.

A transversal angle of incidence of 30° leads to a P_{mpp} of 22 W and an I_{sc} of 1.3 A for both CPC 1 and 2. Lastly, Fig. 28 presents the IV curve at 35° from normal incidence (transversal direction) for the bottom receiver side of geometry CPC 1 and 2.

A P_{mpp} of 20 W and an I_{sc} of 1.2 A, for both CPC 1 and 2, has been achieved at a transversal angle of incidence of 35°. At 25° (Figs. 25 and 26), the I_{sc} drops around −45% as the reflector is no longer able to efficiently reflect the beam radiation. Nevertheless, the decrease in the I_{sc} is sharper in CPC 2 than in CPC 1, possibly due to the section A opening below the bottom receiver side in CPC 1.

5.4. Optical efficiency from thermal measurements

5.4.1. Heat loss coefficient and optical efficiency

Typically, the solar radiation G (W/m^2) reaches the solar module at a certain solar irradiance and a fraction is lost to the ambient as Q_{loss}, then a portion empowers the PV module (Q_{el}) with a given electric efficiency (η_{el}). The accumulation of solar energy increases the temperature of the PV module and generates the thermal power Q_{th}, depending on the HTF and module design, which is transferred to the thermal module through a heat transfer mechanism with a specific thermal efficiency η_{th}. The thermal insulation that is achieved by reducing and eliminating the back and side heat losses will increase the system efficiency. The general electrical and thermal energy equations for a simple PVT module, and overall efficiency (η_{PVT}) can be defined by Eq. (12), Eq. (13) and Eq. (14) [48,49], respectively.

$$\eta_{el} = \frac{Q_{el}}{G_{global} \cdot A_c} \tag{12}$$

$$\eta_{th} = \frac{Q_{th}}{G_{global} \cdot A_c} \tag{13}$$

$$\eta_{PVT} = \eta_{el} + \eta_{th} \tag{14}$$

The main parameter of interest in a ST collector is the optical efficiency η_0 and the heat loss coefficient U_1, which have been plotted in the following Fig. 29, as a function of both HTF and ambient temperature.

From the diagram shown in Fig. 29 the heat loss coefficient U_1, has a value of 5.0 W/m^2.K. Regarding the overall efficiency η_0 of CPC 1, a value of 62.3% (divided in 51.7%$_{th}$ and 10.6%$_{elect}$, $R^2 = 0.997$) has been obtained per gross area. Furthermore, the heat loss coefficient U_1 for CPC 2 (which is given by the slope of the dashed blue line in Fig. 29) reached 5.4 W/m^2.K. Regarding the optical efficiency, a value of 61.8%

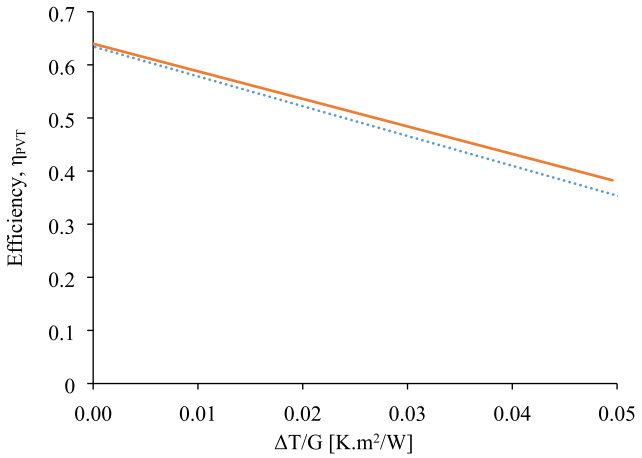

Fig. 29. Experimental overall efficiency per gross area for CPC 1 (solid orange line) and CPC 2 (dashed blue line). (For interpretation of the references to colour in this figure legend, the reader is referred to the web version of this article.)

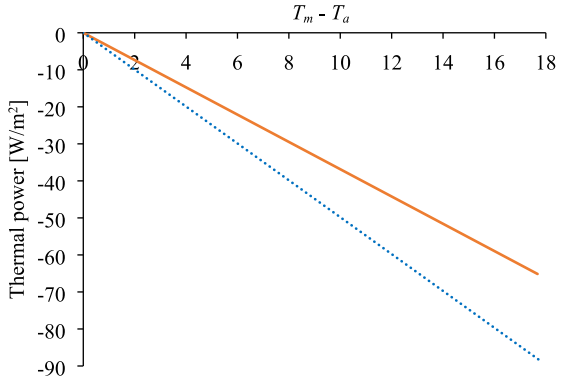

Fig. 30. Experimental heat loss coefficient (dark U-value) per gross area for CPC 1 (solid orange line) and CPC 2 (dashed blue line). (For interpretation of the references to colour in this figure legend, the reader is referred to the web version of this article.)

(divided in 51.2%$_{th}$ and 10.6%$_{elect}$, $R^2 = 0.995$) has been obtained per gross area for CPC 2.

The measured efficiencies are considerably lower than the theoretical efficiencies in Fig. 19, which can be explained by the enhanced optical errors while building the collector, dead areas (e.g. space that it is not actively contributing to the electrical energy production), material

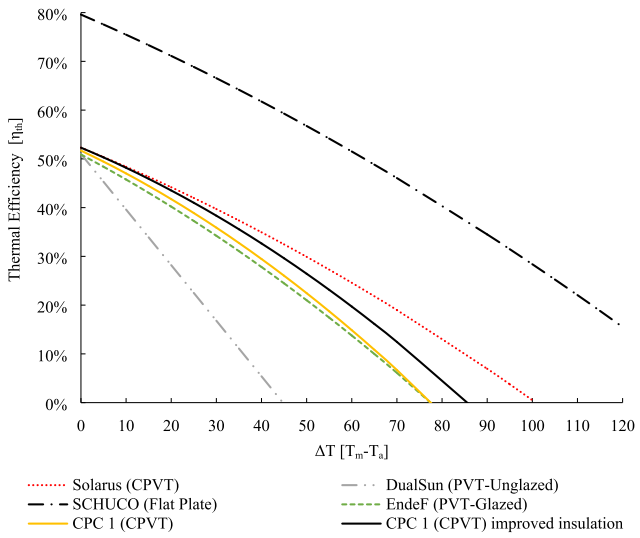

Fig. 31. Comparison of the thermal efficiency arbitrary unglazed (e.g. DualSun), glazed (e.g. EndeF) and low-concentrating (e.g. both Solarus PC and CPC 1 reflector geometry) PVT collectors, and flat-plate ST collectors. Efficiency related to the gross area, at 1000 W/m^2.

absorptance and effective reflectance (e.g. amount of bounces that are required for the light rays to reach the receiver).

Additionally, during nighttime, the dark U-value for each CPC geometry has been drawn, which is presented in the following Fig. 30.

From the diagram shown in Fig. 30, a dark U-value of 3.5 and 4.7 W/m^2.K ($R^2 = 0.999$) has been achieved for both CPC 1 and 2, respectively. As expected, the dark U-value is lower than the U-value obtained from Fig. 29, as during darkness the HTF liquid is warmer than the fin absorber (e.g. low ΔT between the fin and the ambient), thus decreasing the heat losses (i.e. dark U-value < U-value). On the other hand, during illumination, the fin absorber is warmer than the HTF liquid (e.g. bigger ΔT between the fin and the ambient), which leads to higher heat losses (i.e. U-value > dark U-value). The differences between the heat loss coefficient from CPC 1 and 2 can be explained by the higher conduction losses between the bottom receiver side and the reflector material (section A, Fig. 2). Additionally, it is important to state that for a very low ΔT (T_m - T_a) the uncertainty of the measurement increases, nevertheless, it is a good base point to compare both geometries as they have been tested simultaneously.

Overall, the CPC 1 geometry reached a higher optical efficiency (+0.5%$_{rel}$) and at the same time a lower heat loss coefficient of around −8%$_{rel}$ (−0.4 W/m^2.K) than CPC 2. The Solarus PC optical efficiency (per gross area) is around 61.4% (divided in 52.3%$_{th}$ + 9.1%$_{elect}$), which is 5.6% and 4.7% lower than CPC 1 and 2, respectively. Additionally, the Solarus PC has a lower U-value of 3.5 W/m^2.K [33] due to the higher concentration ratio.

The difference between theoretical and measured optical efficiency lies in the incidence angle and on the silicone gel transmittance losses, which will be magnified for high incidence angles, where the difference between the theoretical and measured optical efficiency from I_{sc} measurements is higher.

In addition, a wide-ranging comparison (based on Eq. 10) between several PVT technologies brands (e.g. DualSun, EndeF and Solarus) and an arbitrary flat-plate ST collectors (e.g. Schuco) has been done and presented in the following Fig. 31.

The different collector parameters, such as optical efficiency and heat losses, can be assessed from the Solar Keymark database[1] for each manufacturer and solar collector model, which are presented in the following Table 6.

By improving the insulation, the stagnation temperature of CPC 1 can be further increased from 77 °C to around 85 °C, which leads to higher energy yields at higher temperatures as the ones required for DHW applications. The stagnation temperature of a solar collector is typically achieved when a solar collector is not cooled. One way to decrease the problems that occur while operating the collector at high temperatures is to reduce the HTF temperature and thus reduce the absorber temperature. Moreover, façade integration allows solar collectors to effectively match the solar irradiance in the collector plane to the heat demand for winter, thus reduce the maximum irradiance.

5.5. Electrical incidence angle modifier

From the test method described in Section 4.1 for both transversal and longitudinal electrical IAM, the following section presents an analysis of the results obtained for the electrical IAM$_{Long.}$ and IAM$_{Transv.}$. The IAM factor (for normal incidence) has been acquired by the relation between several parameters, such as the angle of incidence, global irradiation and electrical power. Fig. 32 presents the outdoor testing for both CPC geometries, as well as, for the Solarus PC.

The IAM$_{transv.}$ of the Solarus PC follows the asymmetry of the geometry, where the amount of incoming light into the receiver side facing the reflector decreases from −11° to +37.5° since it is designed to operate at high latitudes. From Fig. 32, it can be seen that the decrease in efficiency is smother in CPC 1 than in CPC 2, possibly due to the opening

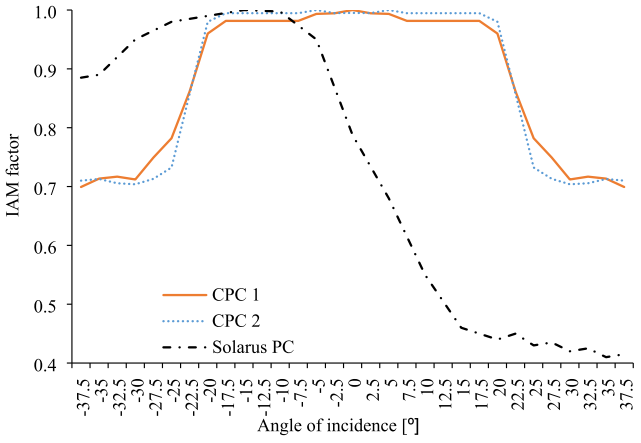

Fig. 32. Normalized experimental electrical transversal IAM for the Solarus PC, CPC 1 and CPC 2.

Table 6
Optical efficiency and heat loss coefficients for several solar collectors, such as CPVT, PVT unglazed, PVT glazed and flat-plat solar thermal collectors.

	CPC 1	CPC 1 improved	Solarus PC	ST flat-plate	PVT Glazed	PVT Unglazed	Unit
η_0	51.7	52.3	52.3	79.6	50.9	51.0	%
c_1	4.4	3.9	3.8	4.0	4.93	11.4	W/m^2 K
c_2	0.029	0.026	0.014	0.011	0.021	–	W/m^2 K^2

[1] https://solarkeymark.eu/database/.

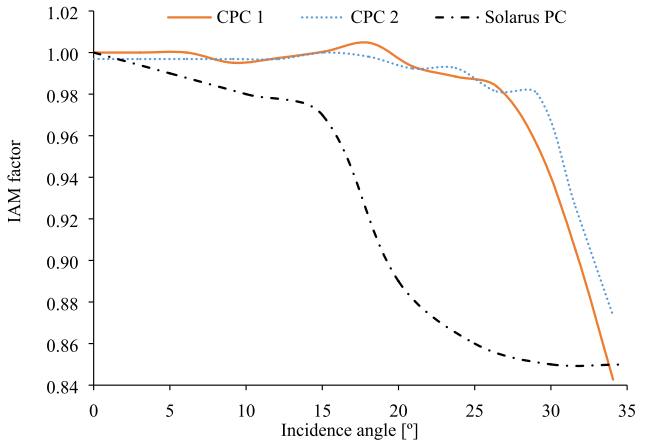

Fig. 33. Normalized experimental electrical longitudinal IAM for the Solarus PC, CPC 1 and CPC 2.

in CPC 1 (section A) that leads some rays to be reflected to the sky. On the other hand, CPC 2 $IAM_{transv.}$ pattern presents a more pronounced decrease in efficiency at the acceptance angle than CPC 1. Furthermore, neither CPC 1 nor CPC 2 have to be dependent on the solar collector tilt angle, as it can be placed as a standard PV module. On the other hand, by having a peak efficiency at −10° the Solarus PC is limited when it comes to collector tilt angle placement. Overall, the CPC geometries show a better performance over the range of the measured incidence angles from −7.5° until +37.5° the IAM factor is considerably higher than the IAM factor of the Solarus PC.

Additionally, the $IAM_{Long.}$ has been measured and compared with the longitudinal electrical IAM of the Solarus PC, being presented in the following Fig. 33.

Fig. 33 presents the incidence angles of the highest importance, therefore incidence angles from 0° until 35° in the longitudinal direction are presented. Due to a longer distance from the bottom receiver to the reflector plate, the Solarus PC has a larger shadow length, therefore leading to a poorer $IAM_{Long.}$ than CPC 1 and 2. Furthermore, it is possible to visualize the importance of the diode system and the PV cell string layout in the overall performance of a photovoltaic system. Fig. 33 clearly shows at which angle of incidence the diode system kicks in, which is around 26° and 29° for CPC 1 and 2 (respectively), and the Solarus PC around 15°. The $IAM_{Long.}$ exposes a weakness of the MaReCo geometry when it comes to shading profiles, as a result of the relatively high distance between the receiver and the reflector plate, which will set the length of the shadow in the bottom receiver side. One way to avoid the significant drop presented previously would be to have a longer reflector, but conversely, the collector will be bigger and not economically viable.

The electrical peak power has been drawn from the IAM measurement procedure, where the top receiver side (facing the sky) reached 52.5 W/m^2 and 51.5 W/m^2 for CPC 1 and 2, respectively. On the other hand, the bottom receiver side (facing the reflector) achieved 65.7 W/m^2 and 65.1 W/m^2 for CPC 1 and 2, respectively. In total, CPC 1 achieved an electrical peak power of 118.2 W/m^2, while CPC 2 achieved 116.6 W/m^2, which are $+8.1\%_{CPC1}$ and $+6.6\%_{CPC2}$ higher than the electrical peak power of the Solarus PC ($P_{el.}$ = 109.7 W/m^2). The Solarus collector electrical peak efficiency is acquired at a tilt angle of −11° (Fig. 33) for an IAM factor of 1.09.

In addition, for the same concentration factor, is expected a higher electrical peak power for the CPC geometries as it 'produces' two focal lines, which allows the reflected rays to be distributed more evenly in the PV cell, and thus decreasing the conduction losses in the PV cell 'fingers'.

Table 7
Normalized longitudinal thermal Incidence Angle Modifier for CPC 1 and Solarus PC solar collector.

Angle of incidence [°]	CPC 1	Solarus PC
0 [+/−1]	1.00	1.00
5 [+/−1]	1.00	1.00
10 [+/−1]	1.00	1.00
15 [+/−1]	1.00	0.99
20 [+/−1]	0.98	0.98
25 [+/−1]	0.98	0.97
30 [+/−1]	0.96	0.96
35 [+/−1]	0.94	0.94
40 [+/−1]	0.92	0.92
45 [+/−1]	0.88	0.89

5.6. Thermal incidence angle Modifier

Additionally, the test method described in Section 4.1 has been applied to access the longitudinal and transversal thermal IAM solely for CPC 1, which is presented in the following Table 7.

Table 7 presents a very steady thermal performance at high incidence angles for both solar collectors, which was expected since the geometry has a minor impact on the thermal $IAM_{Long.}$ performance when compared with the higher impact it has on the $IAM_{transv.}$, as can be seen in Fig. 34.

As expected, the CPC 1 has a better IAM profile than the Solarus PC as the geometry has a high impact on the efficiency of the reflected rays into the bottom receiver side. The acceptance angle is well defined, especially for the CPC 1 reflector geometry. The angles of most importance are comprised between ± 45°, which shows that, as in the transversal electrical IAM, the CPC 1 has an improved reflector geometry and is not limited to specific tilt angles.

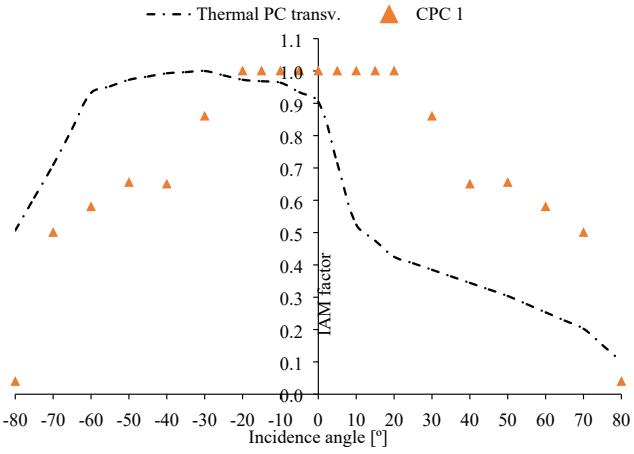

Fig. 34. Normalized transversal thermal Incidence Angle Modifier for the CPC 1 and the Solarus PC solar collector.

Table 8
Summary of the annual weather data used, such as global, direct and diffuse radiation in the horizontal plane, latitude, longitude, standard longitude, average ambient temperature and average wind speed for four different locations.

		Location	
Parameters	Unit	Cairo	Athens
Latitude	–	30° N	38° N
Longitude	–	31° E	23° E
Standard Longitude	–	30°	30°
Global Horizontal Irradiation	kWh/m^2/year	2107	1722
Direct Horizontal Irradiance	kWh/m^2/year	1488	1168
Diffuse Horizontal Irradiance	kWh/m^2/year	619	554
Average ambient temperature	°C	22	18
Average wind speed	m/s	4	5

5.7. Annual electrical and thermal energy yield

The electrical and thermal yields were acquired by means of an in-house simulation tool called CEPT, which was further validated with a minor deviation of around 5% through the Solar Collector Energy Output Calculator (ScenoCalc, version v3.10d: SKN 2011). CEPT is an Excel-based simulation tool that allows the calculation of both electrical and thermal annual energy output. The simulation tool allows the user to input several weather files, which is supported by hourly (time steps) meteorological data records from Meteonorm (Meteonorm, 2018) and are presented in the following Table 8.

The main basis behind CEPT is the assessment of solar collector energy yields over a constant annual HTF temperature (i.e., theoretical maximum achievable collector yield if a constant annual HTF temperature is applied), which assumes an infinite storage capacity (i.e., any heat gain will be utilized).

Table 9
Normalized electrical and thermal input parameters per gross area of each solar collector/module for energy yield assessment.

	CPC 1	Solarus PC	ST flat-plate	PV module	Unit
η_{th}	51.7	52.3	76.1	–	%
$\eta_{th\_diff.}$	40	39	69	–	%
c_1	4.4	3.8	4.4	–	W/m^2 K
c_2	0.029	0.014	0.022	–	W/m^2 K^2
η_{elect}	10.6	9.1	–	19.2	%
$\eta_{elect\_diff.}$	8.2	7	–	17.3	%
β	−0.37	−0.37	–	−0.35	%/°C

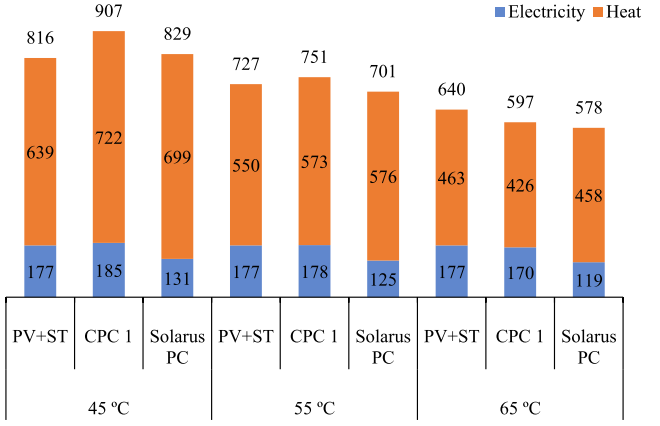

Fig. 35. Annual energy yield (kWh/m^2/year) comparison per square meter for Cairo (30° N; 31° E), Egypt. PV + ST system composed of 0.5 m^2 of PV and 0.5 m^2 of a flat-plate collector. PV module electrical energy yield has been retrieved at 60 °C.

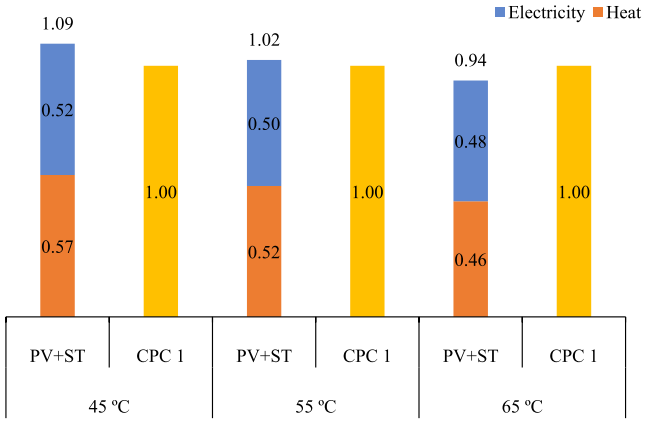

Fig. 36. Required installation area, in m^2, to meet the energy yield production (thermal and electrical) of one square meter of CPC 1 solar collector, for Cairo (30° N; 31° E), Egypt.

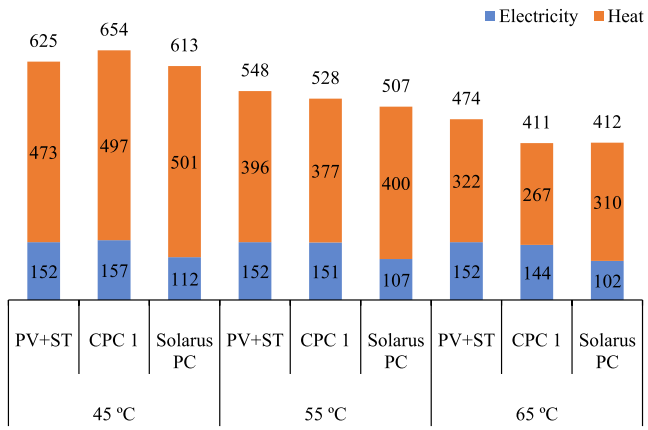

Fig. 37. Annual energy yield (kWh/m^2/year) comparison per square meter for Athens (38° N; 23° E), Greece. PV + ST system composed of 0.5 m^2 of PV and 0.5 m^2 of a flat-plate collector. PV module electrical energy yield has been retrieved at 55 °C.

Input data related to the gross area of each solar collector is required, thus CPC 1, Solarus PC, flat-plate ST collector and PV module main parameters are introduced and presented in the following Table 9.

A comparison between the reflector geometry CPC 1 and the Solarus PC has been performed, as well as with a TrinaSolar TallMax PV module and a Viessmann Vitosol 200FM ST flat-plate solar collector for an installation site located in Cairo is presented in Fig. 35. The PV module electrical energy yield has been retrieved at 55 and 60 °C for Athens and Cairo, respectively. The PV + ST systems and CPC 1 solar collector have been placed with a collector tilt of 25°, whereas the Solarus PC has been installed with a collector tilt of 5° due to its asymmetric reflector geometry.

Electrically, the CPC 1 system outperforms the PC technology for any HTF temperature range, whereas the PV + ST system (which comprises 0.5 m^2 of a PV module and 0.5 m^2 of an ST flat-plate solar collector) is able to keep the performance of the PV module. As the HTF temperature range increases, the CPC 1 thermal annual yield decreases, which falls short from the PV + ST system at temperatures higher than 55 °C. As the presented data suggests, the CPC 1 solar collector outperforms the Solarus PC, therefore the following analysis comprises the required installation area of a PV + ST system to meet the annual energy yield of one square meter of CPC 1 solar collector (Fig. 36).

By combining PV and ST technologies for the same temperature ranges, the PV + ST system requires + 0.09 m^2 (at 45 °C), +0.02 m^2 (at

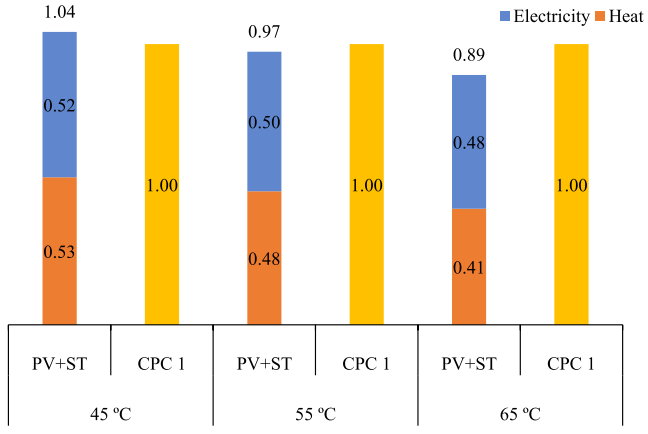

Fig. 38. Required installation area, in m^2, to meet the energy yield production (thermal and electrical) of one square meter of CPC 1 solar collector, for Athens (38° N; 23° E), Greece.

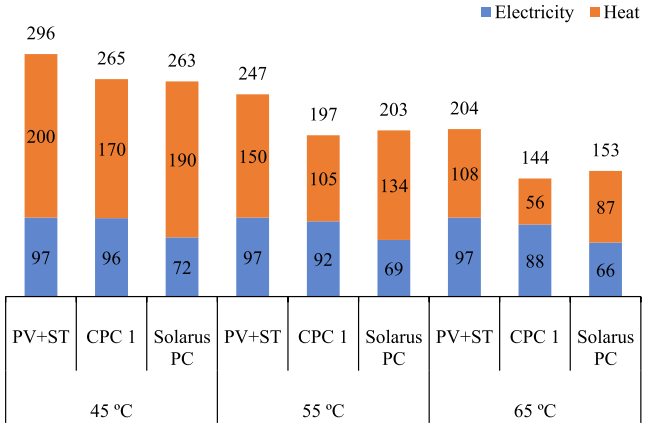

Fig. 39. Annual energy yield (kWh/m^2/year) comparison per square meter for Stockholm (59° N; 18° E), Sweden. PV + ST system composed of 0.5 m^2 of PV and 0.5 m^2 of a flat-plate collector. PV module electrical energy yield has been retrieved at 35 °C.

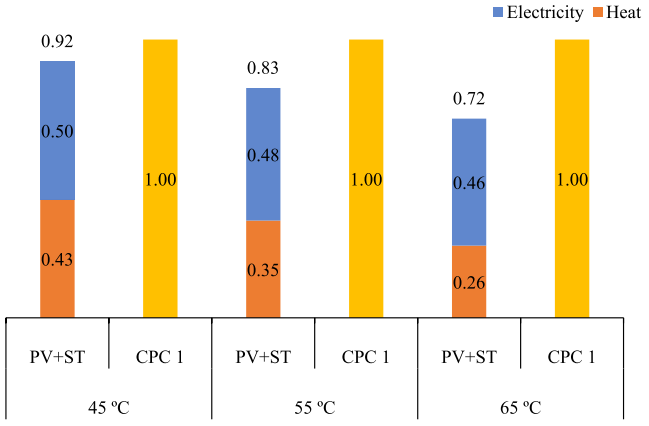

Fig. 40. Required installation area, in m^2, to meet the energy yield production (thermal and electrical) of one square meter of CPC 1 solar collector, for Stockholm (59° N; 18° E), Sweden.

55 °C) and −0.06 m^2 (at 65 °C) to meet both thermal and electrical annual energy yield as the CPC 1 solar collector. Fig. 36 shows that lower temperatures favours the CPVT technology, whereas at high temperatures this advantage in installation area disappears.

A wide variety of radiation profiles are known for different locations, therefore an assessment for different sites has been performed (i.e. for Athens, Stockholm and Cape Town).

In Athens, both the PV + ST system and CPC 1 solar collector have been placed at 35° tilt, whereas the Solarus PC has been installed at 15°. The annual energy yield (kWh/m^2/year) comparison per square meter for Athens is presented in the following Fig. 37.

A CPC 1 collector system, is not able to deliver a higher overall annual energy yield than both PV + ST for temperatures higher than 55 °C. On the other hand, the CPC 1 system is able to outperform, in overall energy yield, the Solarus PC at all ranges of temperatures. On the other hand, the electrical annual yield of a CPC 1 system is fairly similar to the PV + ST system and significantly above the Solarus PC system. Moreover, the required installation area of a PV + ST system to meet the annual energy yield of one square meter of CPC 1 solar collector is presented in Fig. 38.

For an installation site located in Athens, a PV + ST system requires + 0.04 m^2 (at 45 °C), −0.03 m^2 (at 55 °C) and −0.11 m^2 (at 65 °C) than the CPC 1 solar collector to deliver the same annual energy yield, needing fewer square meters of each technology due to its higher efficiencies for 55 °C and 65 °C.

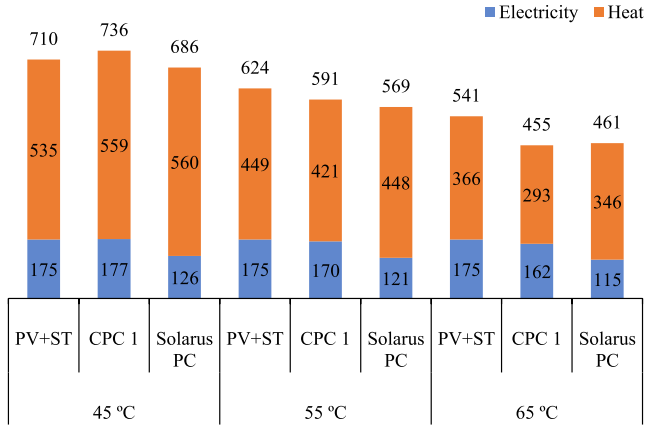

Fig. 41. Annual energy yield (kWh/m^2/year) comparison per square meter for Cape Town (34° S; 18° E), South Africa. PV + ST system composed of 0.5 m^2 of PV and 0.5 m^2 of a flat-plate collector. PV module electrical energy yield has been retrieved at 50 °C.

At high latitudes, as in Stockholm, a system with a higher collector tilt is required, therefore the PV + ST system and CPC 1 solar collector have been placed with a collector tilt of 45°, whereas the Solarus PC has been installed at 25°, in which the annual energy yields registered are shown in Fig. 39.

A CPC 1 collector system, regardless of the HTF temperature range, delivers a higher overall annual energy yield than the Solarus PC, which decreases with an increased HTF temperature range. As expected, the Solarus PC is able to deliver more thermal energy than the CPC 1 collector as its asymmetric reflector geometry copes with the asymmetry of the solar radiation profile at higher latitudes. On the other hand, the electrical production of a CPC 1 system matches the PV + ST system and is almost one-third higher than the Solarus PC system. As seen in the previously, the main difference between the CPC 1 and the PV + ST system lies in the heat conversion factor.

The required installation area of a PV + ST system to meet the annual energy yield of one square meter of CPC 1 solar collector is presented in the following Fig. 40.

In Stockholm, a PV + ST system entails less than −0.08 m^2 (at 45 °C), −0.17 m^2 (at 55 °C) and −0.28 m^2 (at 65 °C) to reach the same thermal and electrical annual yield as the CPC 1 solar collector.

For a system located in Cape Town (Fig. 41), a PV + ST system and CPC 1 solar collector were installed at 30°, whereas the Solarus PC has been placed at a collector tilt of 10°.

A PV + ST system, at HTF temperatures higher than 45 °C, can deliver a higher overall annual energy yield than both CPC 1 and Solarus

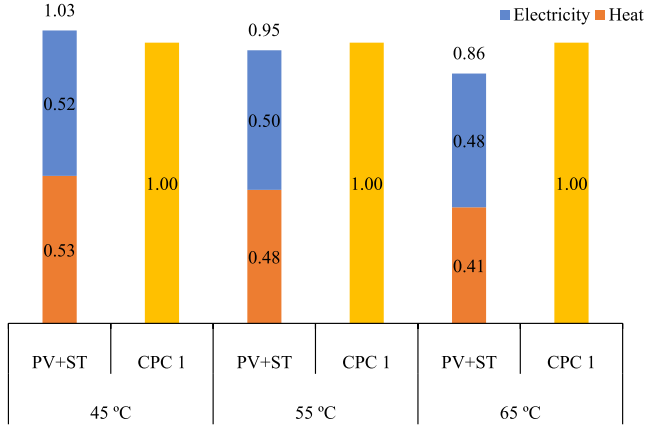

Fig. 42. Required installation area, in m^2, to meet the energy yield production (thermal and electrical) of one square meter of CPC 1 solar collector, for Cape Town (34° S; 18° E), South Africa.

PC. On the other hand, the CPC 1 collector supplies the same electrical energy as the PV + ST system, whereas the PV + ST system achieves higher thermal energy yields, due to its higher heat conversion factor.

A PV + ST system (Fig. 42), for Cape Town, requires + 0.03 m^2 (at 45 °C), −0.05 m^2 (at 55 °C) and −0.14 m^2 (at 65 °C) to deliver the same annual energy yield as the CPC 1 solar system.

It is well established that different locations will provide different ratios between PV + ST and CPVT, which offers a good metric for the technology installation, which will better fit the requirements for energy demand. It is clear that for the given locations the overall best option is a system that comprises both PV and ST technologies since these require fewer square meters of installed area than a CPVT system at higher operating temperatures. At lower operating temperatures, such as 45 °C, the CPVT presents itself as the best solution. The main difference lies in the heat production as the electrical annual yield is fairly similar for both CPC 1 and PV + ST systems regardless of the module temperature. Additionally, a concentrating PVT, such as CPC and Solarus PC, will generate a great portion of electricity and heat per absorber area, but not as much per glazed area. A CPVT system requires almost one-fourth of extra area compared to a PV + ST system, for HTF temperatures higher than 65 °C at the worst location (Stockholm).

Table 10
Present value ratio for different discount rates and operating years.

Year	$d_{3\%}$	$d_{5\%}$	$d_{8\%}$	$d_{11\%}$	$d_{15\%}$	$d_{20\%}$
1	0.97	0.95	0.93	0.90	0.87	0.83
5	4.58	4.33	3.99	3.70	3.35	2.99
10	8.53	7.72	6.71	5.89	5.02	4.19
15	11.94	10.38	8.56	7.19	5.85	4.68
20	14.88	12.46	9.82	7.96	6.26	4.87

5.8. Cost analysis of solar collectors

While sizing a solar system, the cost of solar collectors must be taken into account as it will determine if a specific solar system is viable.

Therefore, a market screening of the available CPVT products has been developed by Lämmle [21], in which different solar collector technologies have been studied such as PV, ST and PVT collectors for the German market.

The market selling price to customers per square meter for an asymmetric CPVT is 250 €/m^2, whereas a PVT-unglazed is around 420 €/m^2 and a PVT-glazed is approximately 455 €/m^2. A monocrystalline PV module price is typically around 142 €/m^2, while a polycrystalline PV module is comprised between 80 and 120 €/m^2. A flat-plate solar collector usually has a cost of 271 €/m^2, while an evacuated tube thermal collector reaches around 465 €/m^2 [21].[2] Surprisingly, the price of an unglazed PVT collector is given by the sum of an average mono-Si PV module and a flat-plate collector.

The current manuscript presented a size-reduction per gross area of −14%, while the height of the CPC 1 collector decreased by –23% (when compared with the asymmetric CPVT Solarus PC), thus fewer raw materials are used by the CPC 1 solar collector. Therefore a lower price can be achieved through a material list breakdown and by applying the required size reductions an estimated cost of 220 €/m^2 can be achieved. Note that the CPC 1 cost prediction is based on the material costs of the asymmetric CPVT of Solarus.

A greater PV module share in a PV + ST system leads to a larger performance gap between systems. The flat-plate installation share sets the PV + ST viability, as the PV module share is fairly constant for a wide

Table 11
Production cost of electrical and thermal energy by a PV module and an ST solar collector in Cairo, for different market discount rates.

Year	*Cost of electrical energy produced in Cairo by a PV module [€/kWh]*						*Cost of thermal energy produced in Cairo at 65 °C by an ST collector [€/kWh]*					
	$d_{3\%}$	$d_{5\%}$	$d_{8\%}$	$d_{11\%}$	$d_{15\%}$	$d_{20\%}$	$d_{3\%}$	$d_{5\%}$	$d_{8\%}$	$d_{11\%}$	$d_{15\%}$	$d_{20\%}$
1	0.83	0.84	0.87	0.89	0.92	0.96	0.60	0.61	0.63	0.65	0.67	0.70
5	0.18	0.19	0.20	0.22	0.24	0.27	0.13	0.14	0.15	0.16	0.17	0.20
10	0.09	0.10	0.12	0.14	0.16	0.19	0.07	0.08	0.09	0.10	0.12	0.14
15	0.07	0.08	0.09	0.11	0.14	0.17	0.05	0.06	0.07	0.08	0.10	0.13
20	0.05	0.06	0.08	0.10	0.13	0.16	0.04	0.05	0.06	0.07	0.09	0.12

Table 12
Production cost of electrical and thermal energy by the CPC 1 solar collector in Cairo, for different market discount rates.

Year	*Cost of electrical energy produced in Cairo [€/kWh]*						*Cost of thermal energy produced in Cairo at 65 °C [€/kWh]*					
	$d_{3\%}$	$d_{5\%}$	$d_{8\%}$	$d_{11\%}$	$d_{15\%}$	$d_{20\%}$	$d_{3\%}$	$d_{5\%}$	$d_{8\%}$	$d_{11\%}$	$d_{15\%}$	$d_{20\%}$
1	1.33	1.36	1.40	1.44	1.49	1.55	0.53	0.54	0.56	0.57	0.59	0.62
5	0.28	0.30	0.32	0.35	0.39	0.43	0.11	0.12	0.13	0.14	0.15	0.17
10	0.15	0.17	0.19	0.22	0.26	0.31	0.06	0.07	0.08	0.09	0.10	0.12
15	0.11	0.12	0.15	0.18	0.22	0.28	0.04	0.05	0.06	0.07	0.09	0.11
20	0.09	0.10	0.13	0.16	0.21	0.27	0.03	0.04	0.05	0.06	0.08	0.11

Table 13
Production cost of electrical and thermal energy by a PV module and an ST solar collector in Cape Town, for different market discount rates.

Year	*Cost of electrical energy produced in Cape Town by a PV module [€/kWh]*						*Cost of thermal energy produced in Cape Town at 65 °C by an ST collector [€/kWh]*					
	$d_{3\%}$	$d_{5\%}$	$d_{8\%}$	$d_{11\%}$	$d_{15\%}$	$d_{20\%}$	$d_{3\%}$	$d_{5\%}$	$d_{8\%}$	$d_{11\%}$	$d_{15\%}$	$d_{20\%}$
1	0.84	0.85	0.88	0.90	0.93	0.97	0.76	0.78	0.80	0.82	0.85	0.89
5	0.18	0.19	0.20	0.22	0.24	0.27	0.16	0.17	0.19	0.20	0.22	0.25
10	0.10	0.11	0.12	0.14	0.16	0.19	0.09	0.10	0.11	0.13	0.15	0.18
15	0.07	0.08	0.09	0.11	0.14	0.17	0.06	0.07	0.09	0.10	0.13	0.16
20	0.05	0.07	0.08	0.10	0.13	0.17	0.05	0.06	0.08	0.09	0.12	0.15

[2] The net list prices, which do not include taxes, are related to the primary energy collector yield.

Table 14
Production cost of electrical and thermal energy by the CPC 1 solar collector in Cape Town, for different market discount rates.

Year	*Cost of electrical energy produced in Cape Town [€/kWh]*						*Cost of thermal energy produced in Cape Town at 65 °C [€/kWh]*					
	$d_{3\%}$	$d_{5\%}$	$d_{8\%}$	$d_{11\%}$	$d_{15\%}$	$d_{20\%}$	$d_{3\%}$	$d_{5\%}$	$d_{8\%}$	$d_{11\%}$	$d_{15\%}$	$d_{20\%}$
1	1.40	1.43	1.47	1.51	1.56	1.63	0.77	0.79	0.81	0.83	0.86	0.90
5	0.30	0.31	0.34	0.37	0.41	0.45	0.16	0.17	0.19	0.20	0.22	0.25
10	0.16	0.18	0.20	0.23	0.27	0.32	0.09	0.10	0.11	0.13	0.15	0.18
15	0.11	0.13	0.16	0.19	0.23	0.29	0.06	0.07	0.09	0.10	0.13	0.16
20	0.09	0.11	0.14	0.17	0.22	0.28	0.05	0.06	0.08	0.09	0.12	0.15

range of HTF temperatures, thus a PV + ST system will always be cheaper (e.g. lower installation costs) at higher HTF temperatures.

Money has different values as it depreciates with time. Therefore, a certain money quantity or cash flow in the future has to be updated accordingly to the current market discount rate (d). A present value ratio taking into account (n) years from the present day can be reduced to its present value by applying the following Eq. (15) [37,50,51].

$$\text{Present value} = \frac{1}{(1 + d)^n} \tag{15}$$

Therefore, Eq. (15) allows the assessment of the true value of the CPC 1 solar collector throughout the next 20 years. The following Table 10 shows the Present value ratio that will be applied in Eq. (16).

To assess the true cost of energy, Eq. (15) can be further developed into the following Eq.16, which takes into account the cost of one unit, Present value and annual energy yield for each technology, respectively.

$$Cost\ of\ energy = \frac{cost\ of\ one\ solar\ collector\ unit}{Annual\ energy\ yield \times Present\ value} \tag{16}$$

The following Tables 11-14 present the assessment of the energy production cost for both PV + ST and CPC 1 solar collectors for different discount rates, PV/ST/CPVT production costs and the number of operating years. The HTF operating temperature has been selected at 65 °C as heat has more value at higher temperatures and in DHW systems the HTF is typically within these HTF temperature ranges.

Tables 11-14 display that the newly developed CPC 1 solar collector requires a higher electrical efficiency, whereas the heat production cost is fairly similar on both CPC 1 and ST solar collectors. The PVT cost breakdown into electricity and heat has not been taken into account, as the author did not find the appropriate approach. Therefore, both heat and electricity production costs were taken at the overall PVT cost production, as 220 €/m^2, which will devalue its energy production cost.

A CPVT system must be further developed in terms of material costs, in which the bifacial PVT receiver is the most costly part of the CPVT solar collector. Additionally, a bifacial PVT receiver comprising PV cells, which are high emitters, could be equipped with a selective surface between PV cells (e.g. filling the 'dead areas') to increase the thermal energy yield by means of higher thermal efficiencies.

From an environmentally perspective, the overall production of c-Si PV modules requires a high intake of fossil fuels from countries such as China and Vietnam, which increase the dependency on non-renewable energy sources. Oppositely, the production of CPC-PVT solar collectors, as a hybrid component, uses less electric energy and less coal power.

6. Conclusion

The measurement results confirmed that both CPC 1 and 2 geometries present a significant improvement from the MaReCo geometry of the Solarus PC for all latitudes investigated. The electrical peak efficiency has been enhanced by 17.7% and 17.3%, for CPC 1 and 2, respectively. Moreover, the electrical peak power improved by 8.1% and 6.6%, for CPC 1 and 2, respectively. The measured optical efficiency increased 5.6% for CPC 1 and 4.7% for CPC 2, which can be translated to 3.5% and 2.5% in thermal peak power for CPC 1 and 2, respectively. The heat loss coefficient for both CPC 1 and 2 increased due to the lower concentration factor.

The IAM profiles showed the biggest improvement of all the parameters that have been measured as CPC 1 and 2 revealed to be less sensitive to high longitudinal incidence angles than the Solarus PC, thus increasing the overall amount of energy production. The results show that CPC 1 solar collector can deliver the same electrical energy yield as the PV + ST system, BY making use of less collector area than the Solarus PC, depending on the HTF temperature range employed.

Moreover, in Cairo, a PV + ST system requires + 0.09 m^2 (at 45 °C), +0.02 m^2 (at 55 °C) and −0.06 m^2 (at 65 °C) to produce the same energy yield, despite the improved IAM and heat loss factor of the CPC 1 solar collector. For Stockholm, the PV + ST system entails −0.08 m^2 (at 45 °C), −0.17 m^2 (at 55 °C) and −0.28 m^2 (at 65 °C), and for Athens, the PV + ST system requires +0.04 m^2 (at 45 °C), −0.03 m^2 (at 55 °C) and −0.11 m^2 (at 65 °C) than the CPC 1 solar collector. In Cape Town, a PV + ST system requires +0.03 m^2 (at 45 °C), −0.05 m^2 (at 55 °C) and −0.14 m^2 (at 65 °C). Furthermore, the improved PVT collector strongly outperforms the Solarus PC in area usage, as it requires less than −0.14 m^2 and thus achieving a lower collector price.

At all ranges of temperatures, the CPC 1 solar collector presents fairly the same electrical annual yield as the PV + ST system, falling short in the thermal energy yield. At low operating HTF temperatures, the CPC 1 solar collector is competitive. The energy performance gap between both technologies decreased, mainly due to the improvements made on the electrical side of the CPC 1 (which considerably outperforms the Solarus PC in both annual electrical and thermal energy yields).

CRediT authorship contribution statement

Diogo Cabral: Methodology, Visualization, Investigation, Writing – original draft, Resources, Supervision, Project administration, Funding acquisition, Validation, Conceptualization, Writing – review & editing.

Declaration of Competing Interest

The authors declare that they have no known competing financial interests or personal relationships that could have appeared to influence the work reported in this paper.

Acknowledgements

This research was partly supported with funding from the European Union's Horizon 2020 research and innovation programme under grant agreement No. 814865 (RES4BUILD) and from the Department of Building Engineering, Energy Systems and Sustainability Science of the University of Gävle. The author is grateful for the fruitful cooperation and support provided by Professor Björn Karlsson during the whole development and reviewing of the manuscript as well as for the input

delivered to develop both Eqs. 3 and 4.

The output reflects only the author's view and the European Union cannot be held responsible for any use that may be made of the information contained therein.

Appendix A

The main outdoor testing results (per gross area) on the CPC-PVT solar collector are presented in the following Table 15. The results present the day and dark heat loss coefficient U_1, thermal and electrical peak efficiency, and electrical and thermal peak power for CPC 1, CPC 2 and the Solarus PC. Moreover, Table 16 presents the annual energy yield for Cairo and Athens for three different solar collector technology systems.

Table 15
Outdoor testing results on the CPC-PVT per gross area.[1]

	Day U_1 [W/m^2.K]	Dark U_1 [W/m^2.K]	Experimental optical efficiency [%]	Thermal peak efficiency [%]	Electrical peak efficiency [%]
CPC 1	5.0	3.5	62.3	51.7	10.61
CPC 2	5.4	4.7	61.8	51.2	10.57
Solarus PC[2]	3.5	–	61.4	52.3	9.1

[1] Coefficient of determination, $R^2 \geq 0.991$.
[2] Solarus (2018).

Table 16
Annual energy yield (kWh/m^2/year) comparison per square meter for Cairo and Athens. PV + ST system composed of 0.5 m^2 of PV and 0.5 m^2 of ST flat-plate solar collector.

	Cairo (30° N; 31° E)			Athens (38° N; 23° E)		
	45 °C	55 °C	65 °C	45 °C	55 °C	65 °C
PV + ST	816	727	640	625	548	474
CPC 1	907	751	597	654	528	411
Solarus PC	829	701	578	613	507	412

References

[1] Qasima U, Imrana H, Kamrana M, Faryad M, Butt N. Computational study of stack/terminal topologies for perovskite based bifacial tandem solar cells. Sol Energy 2020;203:1–9.
[2] Gorouh HA, Salmanzadeh M, Nasseriyan P, Hayati A, Cabral D, Gomes J, et al. Thermal modelling and experimental evaluation of a novel concentrating photovoltaic thermal collector (CPVT) with parabolic concentrator. Renew Energy 2022;181:535–53.
[3] Fraunhofer ISE, 2020. Photovoltaics Report. Updated in 30 October 2020.
[4] Proell M, Karrer H, Brabec CJ, Hauer A. The influence of CPC reflectors on the electrical incidence angle modifier of c-Si cells in a PVT hybrid collector. Sol Energy 2016;126:220–30.
[5] Lämmle M, Oliva A, Hermann M, Kramer K, Kramer W. PVT collector technologies in solar thermal systems: a systematic assessment of electrical and thermal yields with the novel characteristic temperature approach. Sol Energy 2017;155:867–79.
[6] Tomar V, Tiwari GN, Bhatti TS. Performance of different photovoltaic-thermal (PVT) configurations integrated on prototype test cells: An experimental approach. Energy Convers Manage 2017;154:394–419.
[7] Joshi SS, Dhoble AS. Photovoltaic -Thermal systems (PVT): Technology review and future trends. Renew Sustain Energy Rev 2018;92:848–82.
[8] Maatallah T, Zachariah R, Al-Amri FG. Exergo-economic analysis of a serpentine flow type water based photovoltaic thermal system with phase change material (PVT-PCM/water). Sol Energy 2019;193:195–204.
[9] Guarracino I, Freeman J, Ramos A, Kalogirou SA, Ekins-Daukes NJ, Markides CN. Systematic testing of hybrid PV-thermal (PVT) solar collectors in steady-state and dynamic outdoor conditions. Appl Energy 2019;240:1014–30.
[10] Nasseriyan P, Gorouch H, Gomes J, Cabral D, Salmanzadeh M, Lehmann T, et al. Numerical and Experimental Study of an Asymmetric CPC-PVT Solar Collector. Energies 2020;13:1669. https://doi.org/10.3390/en13071669.
[11] Cabral D, Gomes J, Hayati A, Karlsson B. Experimental investigation of a CPVT collector coupled with a wedge PVT receiver. Sol Energy 2021;215:335–45.
[12] Abdullah AL, Misha S, Tamaldin N, Rosl MAM, Sachit FA. Theoretical study and indoor experimental validation of performance of the new photovoltaic thermal solar collector (PVT) based water system. Case Stud Therm Eng 2020;18:100595.
[13] Weiss, Werner, Spörk-Dür, Monika. Solar Heat Worldwide 2020 Edition- Global Market Development and Trends in 2019 - Detailed market Figures 2018; 2020.
[14] IEA SHC, 2018. Task 60. PVT Systems: Application of PVT Collectors and New Solutions in HVAC Systems. Official Description, International Energy Agency Solar Heating and Cooling Programme.
[15] ISO 9806, 2017. ISO 9806:2017 Solar energy - Solar thermal collectors – Test methods.
[16] Jonas D, Lämmle M, Theis D, Schneider S, Frey G. Performance modeling of PVT collectors: Implementation, validation and parameter identification approach using TRNSYS. Sol Energy 2019;193:51–64.
[17] Lämmle M, Herrando M, Ryan G. Basic concepts of PVT collector technologies, applications and markets. Technical Report D.5. IEA SHC Task 60; 2020.
[18] Sathe TM, Dhoble AS. A review on recent advancements in photovoltaic thermal techniques. Renew Sustain Energy Rev 2017;76:645–72. https://doi.org/10.1016/j.rser.2017.03.075.
[19] Kazem HA, Al-Waeli HA, Chaichan MT, Al-Waeli KH, Al-Aasam AB, Sopian K. Evaluation and comparison of different flow configurations PVT systems in Oman: A numerical and experimental investigation. Sol Energy 2020;208:58–88.
[20] George M, Pandey AK, Rahim NA, Tyagi VV, Shahabuddin S, Saidur R. Concentrated photovoltaic thermal systems: A component-by-component view on the developments in the design, heat transfer medium and applications. Energy Convers Manage 2019;186:15–41.
[21] Lämmle M. Thermal Management of PVT Collectors: Development and Modelling of Highly Efficient Glazed, Flat Plate PVT Collectors with Low-Emissivity Coatings and Overheating Protection. Freiburg: Fraunhofer ISE; 2018. PhD thesis.
[22] Lämmle M, Kroyer T, Fortuin S, Wiese M, Hermann M. Development and modelling of highly-efficient PVT collectors with low-emissivity coatings. Sol Energy 2016;130:161–73.
[23] Cabral D, Karlsson B. Electrical and thermal performance evaluation of symmetric truncated C-PVT trough solar collectors with vertical bifacial receivers. Sol Energy 2018;174:683–90. https://doi.org/10.1016/j.solener.2018.09.045.
[24] Lämmle M, Hermann M, Kramer K, Panzer C, Piekarczyk A, Thoma C, et al. Development of highly efficient, glazed PVT collectors with overheating protection to increase reliability and enhance energy yields. Sol Energy 2018;176:87–97.
[25] Tian M, Su Y, Zheng H, Pei G, Li G, Riffat S. A review on the recent research progress in the compound parabolic concentrator (CPC) for solar energy applications. Renew Sustain Energy Rev 2018;82:1272–96. https://doi.org/10.1016/j.rser.2017.09.050.
[26] Reichl Ch, Hengstberger F, Zauner Ch. Heat transfer mechanisms in a compound parabolic concentrator: Comparison of computational fluid dynamics simulations to particle image velocimetry and local temperature measurements. Sol Energy 2013;97:436–46. https://doi.org/10.1016/j.solener.2013.09.003.
[27] Bellos E, Tzivanidis C. Alternative designs of parabolic trough solar collectors. Prog Energy Combust Sci 2019;71:81–117. https://doi.org/10.1016/j.pecs.2018.11.001.
[28] Valizadeh M, Sarhaddi F, Adeli M. Exergy performance assessment of a linear parabolic trough photovoltaic thermal collector. Renew Energy 2019;138:1028–41. https://doi.org/10.1016/j.renene.2019.02.039.
[29] Adam SA, Ju X, Zhang Z, El-samie MMA. Theoretical investigation of different CPVT configurations based on liquid absorption spectral beam filter. Energy 2019;189:116259.
[30] Achkari O, El Fadar A. Latest developments on TES and CSP technologies – Energy and environmental issues, applications and research trends. Appl Therm Eng 2020;167:114806. https://doi.org/10.1016/j.applthermaleng.2019.114806.
[31] Bunthof L, Kreuwel F, Kaldenhoven A, Kin S, Corbeek W, Bauhuis G, et al. Impact of shading on a flat CPV system for façade integration. Sol Energy 2016;7140:162–70.
[32] Kreft W, Przenzak E, Filipowicz M. Photovoltaic chain operation analysis in condition of partial shading for systems with and without bypass diodes. Optik 2021;247:167840. https://doi.org/10.1016/j.ijleo.2021.167840.
[33] Solarus. Technical Brochure of Solarus Power Collector C-PVT and C-T [Brochure]; 2018.
[34] Adsten M, Helgesson A, Karlsson B. Evaluation of CPC-collector designs for stand-alone, roof- or wall installation. Sol Energy 2005;79(6):638–47.
[35] Haedrich I, Eitner U, Wiese M, Wirth H. Unified methodology for determining CTM ratios: systematic prediction of module power. Sol Energy Mater Sol Cells 2014;131:14–23.
[36] IEC 62108, 2007. Concentrator photovoltaic (CPV) modules and assemblies – Design qualification and type approval.
[37] Kalogirou, S.A. 2014. Solar Energy Engineering: Processes and Systems (Second ed.). Academic Press. https://doi.org/10.1016/B978-0-12-374501-9.00014-5.
[38] Coker A. Ludwig's Applied Process Design for Chemical and Petrochemical Plants. 4th ed. Elsevier: Gulf Professional Publishing; 2007.
[39] Carvalho MJ, Collares-Pereira M, Gordon JM, Rabl A. Truncation of CPC solar collectors and its effect on energy collection. Sol Energy 1985;35(5):393–9.
[40] Winston R, Hinterberger H. Principles of cylindrical concentrators for solar energy. Sol Energy 1975;17:255–8.
[41] Cabral D, Gomes J, Karlsson B. Performance evaluation of non-uniform illumination on a transverse bifacial PVT receiver in combination with a CPC geometry. Sol Energy 2019;194:696–708. https://doi.org/10.1016/j.solener.2019.10.069.

[42] Rabl A. Comparison of solar collectors. Sol Energy 1976;18(2):93–111.
[43] Rabl A. Optical and thermal properties of compound parabolic concentrators. Sol Energy 1976;18:497–511.
[44] Collares-Pereira M, O'Gallagher J, Rabl A. Approximations to the CPC-a comment on recent papers by Canning and by Shapiro. Sol Energy 1978;21:245–6.
[45] Rabl A, O'Gallagher J, Winston R. Design and test of non-evacuated solar collectors with compound parabolic concentrators. Sol Energy 1980;25(4):335–51.
[46] Brogen M, Nostell P, Karlsson B. Optical Efficiency of a PV-Thermal Hybrid CPC module for high Latitudes. Sol Energy 2000;69:173–85.
[47] Duffie JA, Beckman WA. Solar Engineering of Thermal Processes. New York: John Wiley & Sons; 2013.
[48] Ramos CAF, Alcaso AN, Cardoso AJM. Photovoltaic-thermal (PVT) technology: Review and case study. Proceedings of the IOP Conference Series: Earth and Environmental Science; IOP Publishing; 2019, 354, 12048.
[49] Shakouri M, Ebadi H, Gorjian S. Solar photovoltaic thermal (PVT) module technologies. Photovoltaic Solar Energy Conversion Elsevier 2020:79–116.
[50] Singh DB, Tiwari GN. Energy, exergy and cost analyses of N identical evacuated tubular collectors integrated basin type solar stills: A comparative study. Sol Energy 2017;155:829–46. https://doi.org/10.1016/j.solener.2017.07.018.
[51] Singh DB, Tiwari GN. Exergoeconomic, enviroeconomic and productivity analyses of basin type solar stills by incorporating N identical PVT compound parabolic concentrator collectors: A comparative study. Energy Convers Manage 2017;135:129–47. https://doi.org/10.1016/j.enconman.2016.12.039.